

# The Age–Metallicity–Specific Orbital Energy Relation for the Milky Way’s Globular Cluster System Confirms the Importance of Accretion for Its Formation

TURNER WOODY<sup>1</sup> AND KEVIN C. SCHLAUFMAN<sup>1</sup>

<sup>1</sup>*Department of Physics and Astronomy  
Johns Hopkins University  
3400 N Charles St  
Baltimore, MD 21218, USA*

(Received October 23, 2020; Revised March 23, 2021; Accepted April 11, 2021)

Accepted for publication in the *Astronomical Journal*

## ABSTRACT

Globular clusters can form inside their host galaxies at high redshift when gas densities were higher and gas-rich mergers were common. They can also form inside lower-mass galaxies that have since been accreted and tidally disrupted, leaving their globular cluster complement bound to higher-mass halos. We argue that the age–metallicity–specific orbital energy relation in a galaxy’s globular cluster system can be used to identify its origin. Gas-rich mergers should produce tightly bound systems in which metal-rich clusters are younger than metal-poor clusters. Globular clusters formed in massive disks and then scattered into a halo should have no relationship between age and specific orbital energy. Accreted globular clusters should produce weakly bound systems in which age and metallicity are correlated with each other but inversely correlated with specific orbital energy. We use precise relative ages, self-consistent metallicities, and space-based proper motion-informed orbits to show that the Milky Way’s metal-poor globular cluster system lies in a plane in age–metallicity–specific orbital energy space. We find that relatively young or metal-poor globular clusters are weakly bound to the Milky Way, while relatively old or metal-rich globular clusters are tightly bound to the Galaxy. While metal-rich globular clusters may be formed either in situ or ex situ, our results suggest that metal-poor clusters formed outside of the Milky Way in now-disrupted dwarf galaxies. We predict that this relationship between age, metallicity, and specific orbital energy in a  $L^*$  galaxy’s globular cluster system is a natural outcome of galaxy formation in a  $\Lambda$ CDM universe.

*Keywords:* Galaxy formation(595) — Globular star clusters(656) — Milky Way dynamics(1051) — Milky Way Galaxy(1054) — Milky Way formation(1053) — Milky Way stellar halo(1060)

## 1. INTRODUCTION

Globular cluster formation is one the enduring unsolved problems in astrophysics. Globular clusters can form either in situ inside their parent galaxy or ex situ in lower-mass galaxies that have been accreted and tidally disrupted by a more massive halo (e.g., West et al. 2004; Forbes et al. 2018). In either case, the ancient ages inferred for most globular clusters indicate that they formed long ago when the universe was very dif-

ferent from its current  $z = 0$  state. Indeed, the interval spanning the 16th and 84th percentiles of the Milky Way globular cluster system’s age distribution is 11 Gyr  $\lesssim \tau \lesssim$  13 Gyr or  $2.4 \lesssim z \lesssim 7.3$  in terms of redshift (e.g., Marín-Franch et al. 2009; VandenBerg et al. 2013; Wright 2006). Both in situ and ex situ formation channels are theoretically expected to contribute to the Milky Way’s globular cluster system (e.g., Griffen et al. 2010; Renaud et al. 2017).

In the in situ formation scenario, globular clusters form inside their parent galaxy in gas-rich galaxy mergers (e.g., Ashman & Zepf 1992; Muratov & Gnedin 2010; Li & Gnedin 2014, 2019; Kim et al. 2018) and/or in gas-rich disks (e.g., Kravtsov & Gnedin 2005; Kruijssen

Corresponding author: Turner Woody  
twody1@jhu.edu

2015; Pfeffer et al. 2018; Keller et al. 2020). Galaxies in general and galaxies destined to be similar to the Milky Way in particular are observed to be smaller at high redshift when globular clusters form in this scenario (e.g., Patel et al. 2013a,b). Consequently, globular clusters formed in this way should be tightly bound to their now more-massive and larger parent galaxies at  $z = 0$  (e.g., Leaman et al. 2013). Another robust prediction of the gas-rich merger scenario is that metal-rich clusters should be systematically younger than metal-poor clusters (Li & Gnedin 2014, 2019).

In the ex situ scenario, globular clusters form outside their  $z = 0$  host halo in parent galaxies that have since been accreted and tidally disrupted (e.g., Searle & Zinn 1978; Mackey & Gilmore 2004; Forbes & Bridges 2010; Forbes 2020; Massari et al. 2019). While in most cases it is difficult to conclusively associate a candidate accreted globular cluster with its parent galaxy, the globular clusters Arp 2, NGC 6715 (M 54), Pal 12, Terzan 7, and Terzan 8 have all been securely associated with the Sagittarius dwarf spheroidal (dSph) galaxy (e.g., Law & Majewski 2010; Sohn et al. 2018). Given the collisionless nature of their accretion, globular clusters formed ex situ should be on average less tightly bound to their host galaxy at  $z = 0$  than clusters formed in situ in gas-rich conditions.

The observed properties of accreted globular clusters can be used to set limits on the properties of their parent galaxies. Likewise, the ensemble properties of a galaxy’s accreted globular cluster system can be used to explore its formation. The maximum metallicity realized in a dwarf galaxy’s globular cluster system should not exceed the dwarf galaxy’s typical metallicity. This is the case in both the Fornax and Sagittarius dSph galaxies. The Fornax dSph has  $\langle[\text{Fe}/\text{H}]\rangle = -1.04$  (Kirby et al. 2013), while its five globular clusters span the range  $-2.5 \lesssim [\text{Fe}/\text{H}] \lesssim -1.4$  (e.g., Letarte et al. 2006; Larsen et al. 2012). While the Sagittarius dSph has  $\langle[\text{Fe}/\text{H}]\rangle \approx -0.5$  (e.g., Chou et al. 2007; Hasselquist et al. 2017), the five globular clusters securely associated with it span the metallicity range  $-2.3 \lesssim [\text{Fe}/\text{H}] \lesssim -0.6$  (e.g., Cohen 2004; Sbordone et al. 2007; Mottini et al. 2008; Carretta et al. 2010, 2014). A lower limit on the stellar mass of a galaxy necessary for the formation of a globular cluster of a given metallicity can therefore be derived from a stellar mass–metallicity relationship. Kirby et al. (2013) showed that there exists a linear relationship between log stellar mass and metallicity for dwarf galaxies over five orders of magnitude such that the typical metallicity of a dwarf galaxy rises linearly with log stellar mass from  $[\text{Fe}/\text{H}] \approx -2.5$  at  $M_* \sim 10^3 M_\odot$  to  $[\text{Fe}/\text{H}] \approx -1.0$  at  $M_* \sim 10^8 M_\odot$ . So while both metal-

rich and metal-poor globular clusters can form in massive dSph galaxies, low-mass dSph galaxies will only be able to form metal-poor clusters. More sophisticated arguments based on cosmological dark matter-only or hydrodynamical simulations have reached similar conclusions (e.g., Choksi et al. 2018; Kruijssen 2019; Kruijssen et al. 2019a,b).

The mass of an accreted globular cluster’s parent galaxy will also affect its orbit. A dwarf galaxy orbiting inside the dark matter halo of a more massive galaxy will lose angular momentum due to dynamical friction and its orbit will decay on a timescale that is proportional to its mass (e.g., Binney & Tremaine 2008). Massive dSph galaxies will therefore be dragged into the inner regions of their host halo and tidally disrupted much more quickly than low-mass dSph galaxies. In particular, a massive dSph galaxy resembling Fornax with a total mass  $M_{\text{tot}} \sim 10^8 M_\odot$  capable of forming a globular cluster with  $[\text{Fe}/\text{H}] \approx -1.0$  will be tidally disrupted 100 times faster than a low-mass dSph galaxy with a total mass  $M_{\text{tot}} \sim 10^6 M_\odot$  that could not form a globular cluster more metal-rich than  $[\text{Fe}/\text{H}] \approx -2.0$  (e.g., Pascale et al. 2018; Simon 2019). The metal-rich globular clusters deposited deep inside the more massive halo when their parent massive dSph galaxy is tidally disrupted will be much more tightly bound to the massive halo than any metal-poor globular clusters left behind when their parent low-mass dSph galaxy is tidally disrupted much later.

The ages of accreted globular clusters should be related to the masses and therefore the metallicities of their parent galaxies too. In similar environments, galaxies destined to be massive form in higher  $\sigma$  peaks in the primordial matter density distribution than galaxies destined to be low mass (e.g., Mo et al. 2010). Since the dynamical time  $t_{\text{dyn}}$  scales like  $t_{\text{dyn}} \propto \rho^{-1/2}$ , in similar environments more massive galaxies form stars earlier and therefore the ages of the oldest stellar populations in galaxies should be correlated with their masses. The implication is that in similar environments the age of the oldest globular cluster formed in a dwarf galaxy should be correlated with its mass. This is the case for the  $M_{\text{tot}} \approx 9 \times 10^7 M_\odot$  Fornax dSph galaxy, the  $M_{\text{tot}} \gtrsim 4 \times 10^8 M_\odot$  Sagittarius dSph galaxy, and the  $M_{\text{tot}} \sim 10^{11} M_\odot$  Large Magellanic Cloud (e.g., Pascale et al. 2018; Vasiliev & Belokurov 2020; Erkal et al. 2019). The Fornax globular clusters 1, 3, and 5 are comparable in age to NGC 4590 (M 68) while cluster 4 is somewhat younger (e.g., Buonanno et al. 1998, 1999). On the other hand, Terzan 8 is the oldest globular cluster with a confirmed Sagittarius association and is older than NGC 4590 (e.g., Marín-Franch et al. 2009; Sohn

et al. 2018). Likewise, the oldest of the Large Magellanic Cloud’s globular clusters that are not affected by crowding, Hodge 11, is older than Terzan 8 but younger than the Milky Way’s oldest globular clusters (Wagner-Kaiser et al. 2017). Analyses based on scaling relations calibrated with cosmological hydrodynamical simulations reach similar conclusions (e.g., Kruijssen 2019).

The relationship between age and metallicity in the Galaxy’s globular cluster system has long been used to constrain Milky Way formation. As we described above, analyses of the relationship between age, metallicity, and orbital properties in the Milky Way’s globular cluster system can be even more informative. If globular clusters formed in situ are produced in gas-rich mergers, then metal-rich clusters should be younger than metal-poor clusters and both metal-rich and metal-poor clusters should be relatively tightly bound to their parent galaxy. If globular clusters are formed in situ in gas-rich disks and subsequently scattered into the halo, then there should be no relationship between age and specific orbital energy. In the ex situ formation and accretion scenario, older, metal-rich globular clusters should be tightly bound to their  $z = 0$  host galaxies while younger, metal-poor globular clusters should be weakly bound to their  $z = 0$  host. These straightforward arguments have been confirmed by cosmological hydrodynamical simulations (e.g., Pfeffer et al. 2020).

In this paper, we calculate the orbits of the Milky Way’s globular clusters with precise space-based astrometry. We use those orbits along with precise relative ages and metallicities from the literature to quantify the relationship between age, metallicity, and specific orbital energy in the Milky Way’s globular cluster system. We describe the construction of our globular cluster sample in Section 2. We detail in Section 3 our orbital integrations and statistical analyses of the age–metallicity–specific orbital energy relation in our complete sample of globular clusters as well as its metal-rich/metal-poor subsamples. We review our results and their implications for the formation of the Milky Way’s globular cluster system specifically and globular cluster formation in general in Section 4. We conclude by summarizing our findings in Section 5.

## 2. DATA

In an analysis of the age–metallicity–specific orbital energy relation in the Milky Way’s globular cluster system, the limiting factors are precise cluster ages and proper motions. Most of our proper motion measurements come from Gaia Data Release 2 (DR2; Gaia Collaboration et al. 2016, 2018b,a; Crowley et al. 2016; Fabricius et al. 2016; Arenou et al. 2018; Hambly et al.

2018; Lindegren et al. 2018; Luri et al. 2018). We supplement the globular cluster proper motions published in Gaia Collaboration et al. (2018a) with the Gaia DR2-based proper motions for NGC 6584 and NGC 6723 from Baumgardt et al. (2019) that have proper motion precisions  $\mu/\sigma_\mu > 85$ .<sup>1</sup> We also add proper motions measurements for NGC 1261, NGC 4147, NGC 6101, Terzan 7, Arp 2, Terzan 8, NGC 6934, and Pal 12 from the High-resolution Space Telescope Proper Motion Collaboration (HSTPROMO; Sohn et al. 2018). We list our input globular cluster proper motions in Table 1.

Globular cluster age determinations are inherently difficult to put on an absolute age scale and can be non-trivially affected by even small differences in analysis techniques. Since the analyses we will describe in Section 3 only make use of relative age differences, we choose to use the homogeneous relative globular cluster ages presented in Marín-Franch et al. (2009) to avoid the difficulties associated with absolute ages. Marín-Franch et al. (2009) calculated relative clusters ages  $\tau = \text{age}/12.8$  Gyr for two different metallicity scales (Zinn & West 1984; Carretta & Gratton 1997) as reported in Rutledge et al. (1997a,b) and four different sets of theoretical stellar models (Bertelli et al. 1994; Girardi et al. 2000; Pietrinferni et al. 2004; Dotter et al. 2007). We list our adopted globular cluster metallicities and normalized ages in Table 2. While we focus on the relative ages calculated assuming the more modern Carretta & Gratton (1997) metallicity scale and Dotter et al. (2007) models given in Table 2, the analysis we describe in Section 3 reaches the same conclusion regardless of the assumed metallicity scale or model grid.

We adopt the globular cluster distances and radial velocities listed in Table 1 from the December 2010 revision of the Harris (1996) compilation.<sup>2</sup> Since the December 2010 revision of the Harris (1996) compilation does not provide uncertainties for its distance estimates, we estimate distance uncertainties by first transforming the distance inferences into distance moduli. We next assume a uniform distance modulus uncertainty of 0.05 mag and sample each cluster’s distance modulus from a normal distribution centered on its distance modulus with standard deviation 0.05 mag. We then transform the simulated distance moduli calculated in this way back into distances and uncertainties. We will use the 57 Milky Way globular clusters listed in Tables 1 and 2 with homogeneous relative ages and metallicities plus

<sup>1</sup> We use this threshold because all of the globular cluster proper motions from Gaia Collaboration et al. (2018a) have  $\mu/\sigma_\mu > 85$  in the Baumgardt et al. (2019) catalog.

<sup>2</sup> <https://physwww.mcmaster.ca/~harris/mwgc.ref>

precise space-based proper motions to explore the relationship between age, metallicity, and specific orbital energy in Section 3.

### 3. ANALYSIS

We use the right ascensions  $\alpha$ , declinations  $\delta$ , proper motions  $\mu_\alpha$  &  $\mu_\delta$ , distances  $d$ , and radial velocities  $v_r$  given for the 57 globular clusters listed in Table 1 to calculate their orbits and specific orbital energies. We use a Monte Carlo approach to average over the uncertainties in our input proper motions, distances, and radial velocities. On each iteration, we sample the necessary input data for an orbit integration ( $\alpha$ ,  $\delta$ ,  $\mu_\alpha$ ,  $\mu_\delta$ ,  $d$ , and  $v_r$ ) from the data and uncertainties in Table 1. When possible, we account for the covariance between simultaneously inferred proper motion and parallax inferences. For the globular clusters with proper motions from Gaia Collaboration et al. (2018a), we account for the covariance between proper motions and parallaxes even though we use Harris (1996)-based distances instead of the Gaia DR2 parallax-based distances. For the globular clusters with proper motions from Baumgardt et al. (2019), we account for the covariance between the proper motion components. Sohn et al. (2018) did not provide estimates of the covariance between proper motion components, so we sample each proper motion component independently from within its quoted uncertainty. For distances and radial velocities, we sample from normal distributions with the means and standard deviations given in Table 1. We repeat this process 100 times to generate 100 sets of initial conditions for each globular cluster.

For each Monte Carlo initial condition realization, we integrate a cluster’s orbit in model Milky Way potentials using the `galpy` python module<sup>3</sup> (Bovy 2015). We calculate orbits from the present five Gyr into the past with a time step of 200,000 years assuming a solar motion with respect to the local standard of rest ( $U_\odot$ ,  $V_\odot$ ,  $W_\odot$ ) = (11.1, 12.24, 7.25) km s<sup>-1</sup> (e.g., Schönrich et al. 2010).

We calculate orbits in three different model Milky Way potentials: the default `MWPotential2014` from Bovy (2015), a scaled version of `MWPotential2014` with its halo mass increased by 50%, and `McMillan17` from McMillan (2017). In the default `MWPotential2014` potential, the virial mass and radius are  $M_{\text{vir}} = 0.8 \times 10^{12} M_\odot$  and  $r_{\text{vir}} = 245$  kpc respectively. Its bulge is parameterized as a power-law density profile with exponent  $-1.8$  that is exponentially cut-off at 1.9 kpc. Its

disk is represented by a Miyamoto–Nagai potential with a radial scale length of 3 kpc and a vertical scale height of 280 pc (Miyamoto & Nagai 1975). Its halo is modeled as a Navarro–Frenk–White (NFW) halo with a scale length of 16 kpc (Navarro et al. 1996). The scaled version of the `MWPotential2014` potential differs from the default `MWPotential2014` potential in that we have increased its halo mass by 50%. This change increases the virial mass to  $M_{\text{vir}} = 1.2 \times 10^{12} M_\odot$ . In both cases, we set the solar distance to the Galactic center to  $R_0 = 8.122$  kpc, the circular velocity at the Sun to  $V_0 = 238$  km s<sup>-1</sup>, and the height of the Sun above the plane to  $z_0 = 25$  pc (Jurić et al. 2008; Bland-Hawthorn & Gerhard 2016; Gravity Collaboration et al. 2018).

The `McMillan17` potential has  $M_{\text{vir}} = 1.4 \times 10^{12} M_\odot$ . Its bulge is parameterized as a spherical power law density profile with exponent  $-1.8$  that is finite at  $r = 0$  and has an exponential cut-off at 2.1 kpc. Its disk is split into four components: a thin stellar disk, a thick stellar disk, an H I gas disk, and an H<sub>2</sub> gas disk. Its two stellar disks are modeled as exponential in both the cylindrical radius  $R$  and height  $z$ , with scale lengths  $R_{\text{d,thin}} = 2.6$  kpc,  $R_{\text{d,thick}} = 3.6$  kpc,  $z_{\text{d,thin}} = 300$  pc, and  $z_{\text{d,thick}} = 900$  pc. Its two gas disks are modeled as exponential in  $R$  with a central hole and a modified exponential profile in the  $z$  coordinate. Its halo is modeled as a NFW halo with a scale length of 19.6 kpc. The `McMillan17` potential uses a solar distance and circular velocity of 8.21 kpc and 233.1 km s<sup>-1</sup>.

The Milky Way’s mass within 25 kpc  $M_{25}$  is especially relevant for this problem, and estimates of  $M_{25}$  for the Milky Way based on globular cluster kinematics suggest that  $M_{25} \approx 0.26_{-0.06}^{+0.10} \times 10^{12} M_\odot$  (Eadie & Jurić 2019). The  $M_{25}$  values for the default `MWPotential2014`, the scaled `MWPotential2014`, and the `McMillan17` potentials are  $M_{25} = 0.25 \times 10^{12} M_\odot$ ,  $M_{25} = 0.29 \times 10^{12} M_\odot$ , and  $M_{25} = 0.28 \times 10^{12} M_\odot$  respectively. All three potentials are therefore consistent the best available Milky Way constraints in the same volume. While both the default `MWPotential2014` and `McMillan17` potentials are generally consistent with literature estimates of the Milky Way’s virial mass, most recent mass estimates making use of Gaia DR2 proper motions suggest virial masses in the range  $1.1 \times 10^{12} M_\odot \lesssim M_{\text{vir}} \lesssim 1.4 \times 10^{12} M_\odot$  (e.g., Wang et al. 2020). While the virial mass of the `McMillan17` potential is in this interval, the virial mass of the default `MWPotential2014` potential is below this range. In addition, the `McMillan17` potential provides a more comprehensive model of the Milky Way’s disk than either the default or scaled `MWPotential2014` potentials. This difference could be important for the relatively nearby clusters that dom-

<sup>3</sup> <https://github.com/jobovy/galpy>



inate our input sample. For all of these reasons, the `McMillan17` potential likely provides a better approximation to the true Milky Way potential than the default and scaled `MWPotential2014` potentials.

Our orbit integrations produce 100 plausible orbits for each of the 57 globular clusters listed in Table 1 in the default `MWPotential2014`, scaled `MWPotential2014`, and `McMillan17` potentials. We calculate the 16th, 50th, and 84th percentiles of the specific orbital energy (SOE) distribution for every cluster and use those data to define each cluster’s specific orbital energy and uncertainty in each potential. We list the specific orbital energies derived in this way for each cluster in Table 2.

We use the `statsmodels` python module (Seabold & Perktold 2010) to fit an ordinary least squares linear regression of the form  $\text{SOE} = \beta_0 + \beta_\tau\tau + \beta_M[\text{M}/\text{H}]$  to the age–metallicity–specific orbital energy distribution produced by each set of initial conditions in all three potentials. We aggregate the results and calculate the 16th, 50th, and 84 percentiles of each distribution. We report the results in Table 3. In all three potentials, we find evidence of an age–metallicity–specific orbital energy relationship in which relatively old, metal-rich globular clusters have more negative specific orbital energies and are therefore more tightly bound to the Milky Way than relatively metal-poor, young globular clusters. This relationship is especially strong in the `McMillan17` potential, as  $\beta_\tau$  and  $\beta_M$  in that potential are significant at approximately the 5- $\sigma$  level.

We separately study the age–metallicity–specific orbital energy relationship for metal-rich and metal-poor clusters. We split the complete sample into metal-rich/metal-poor subsamples at  $[\text{M}/\text{H}] = -0.8$  because that cleanly separates the two peaks of the complete sample’s bimodal metallicity distribution. We find similar results for both the complete sample and the metal-poor subsample of globular clusters that we define as the 45 globular clusters with  $[\text{M}/\text{H}] \leq -0.8$ . The  $t$  values and therefore the statistical significances of the coefficients defining the relation are generally larger in absolute value for the metal-poor subsample. For the 12 metal-rich clusters with  $[\text{M}/\text{H}] > -0.8$ , the age–metallicity–specific orbital energy relationship is much weaker. Indeed, if we exclude the two metal-rich globular clusters associated with the Sagittarius dSph, then in both the default and scaled `MWPotential2014` potentials the coefficients defining the age–metallicity–specific orbital relation energy change signs such that older, more metal-rich clusters are less tightly bound to the Milky Way. In this case, there is no significant age–metallicity–specific orbital energy relationship for the `McMillan17` potential.

We use  $F$  tests to compare the full age–metallicity–specific orbital energy model we derived above with each of its nested submodels to verify that the full age–metallicity–specific orbital energy model best describes the data in Table 2. For each subsample in each potential, we tested three null hypotheses:  $\beta_\tau = 0$ ,  $\beta_M = 0$ , and  $\beta_\tau = \beta_M = 0$ . We report the results of those model comparisons in Table 4. For the metal-poor subsample in all three potentials, the  $p$  values for each test are small enough to confidently reject the null hypotheses. The implication is that the full linear model is a better description of the metal-poor subsample than any of its nested submodels. In the case of the `McMillan17` potential, the full linear model is a better description of the complete sample than any of its nested submodels. On the other hand, for the metal-rich subsample there is no reason to prefer the full age–metallicity–specific orbital energy model over any of its nested submodels. We also use the Bayesian information criterion (BIC) to compare models. Smaller BIC values indicate better models, and the results in Table 5 show that the full age–metallicity–specific orbital energy model is preferred to any of its nested submodels for both the complete sample and metal-poor subsample in the `McMillan17` potential. All models are approximately similar in the default and scaled `MWPotential2014` potentials.

We plot the distribution of the Milky Way’s globular cluster systems in the age–metallicity–specific orbital energy space for all three potentials in Figure 1. It is clear that the 57 globular clusters listed in Tables 1 and 2 lie in a plane in age–metallicity–specific orbital energy space in the `McMillan17` potential, exactly as predicted by our linear modeling. We plot two-dimensional projections of age–metallicity–specific orbital energy space for the default `MWPotential2014`, scaled `MWPotential2014`, and `McMillan17` potentials in Figures 2, 3, and 4. There remains significant dispersion about the linear model visualized in Figures 2, 3, and 4, so the age–metallicity–specific orbital energy relation inference we described in Section 1 does not fully explain the highly nonlinear process of globular cluster formation. Nevertheless, the meaningfully non-zero  $R^2$  values presented in Table 3 show that a simple three-parameter linear model explains at least 15%—and possibly as much as 38%—of the variance in the metal-poor globular cluster age–metallicity–specific orbital energy relation.

#### 4. DISCUSSION

We find a significant age–metallicity–specific orbital energy relationship for the metal-poor subsample of 45 globular clusters with  $[\text{M}/\text{H}] \leq -0.8$  listed in Tables

**Table 3.** Median Regression Model Coefficients and  $t$  Values

Sample	$\beta_0$	$\beta_0$	$\beta_\tau$	$\beta_\tau$	$\beta_M$	$\beta_M$	$R^2$
	( $10^4$ )	$t$ Value	( $10^4$ )	$t$ Value	( $10^4$ )	$t$ Value	
<b>Default MWPotential2014</b>							
Complete	$-5.39 \pm 2.32$	-2.33	$-4.12 \pm 2.54$	-1.62	$-1.16 \pm 0.63$	-1.84	0.081
Metal-poor	$-2.21 \pm 3.07$	-0.72	$-8.64 \pm 3.62$	-2.39	$-1.98 \pm 0.92$	-2.16	0.146
Metal-rich <sup>a</sup>	$-11.26 \pm 5.19$	-2.17	$-1.38 \pm 4.20$	-0.33	$-7.45 \pm 8.09$	-0.92	0.087
Metal-rich <sup>b</sup>	$-22.52 \pm 10.02$	-2.25	$19.30 \pm 10.80$	1.79	$9.34 \pm 10.16$	0.92	0.317
<b>Scaled MWPotential2014</b>							
Complete	$-10.17 \pm 2.44$	-4.16	$-3.95 \pm 2.68$	-1.47	$-1.40 \pm 0.67$	-2.10	0.089
Metal-poor	$-5.89 \pm 3.19$	-1.85	$-9.53 \pm 3.76$	-2.54	$-2.15 \pm 0.95$	-2.26	0.160
Metal-rich <sup>a</sup>	$-18.20 \pm 5.42$	-3.36	$-0.12 \pm 4.38$	-0.03	$-9.53 \pm 8.46$	-1.13	0.131
Metal-rich <sup>b</sup>	$-30.52 \pm 9.72$	-3.14	$22.91 \pm 10.48$	2.19	$9.52 \pm 9.85$	0.97	0.407
<b>McMillan17</b>							
Complete	$1.39 \pm 3.95$	0.35	$-24.52 \pm 4.33$	-5.66	$-4.85 \pm 1.08$	-4.49	0.435
Metal-poor	$2.80 \pm 5.23$	0.54	$-28.18 \pm 6.17$	-4.57	$-6.32 \pm 1.56$	-4.05	0.381
Metal-rich <sup>a</sup>	$-3.86 \pm 9.24$	-0.42	$-24.76 \pm 7.47$	-3.32	$-15.79 \pm 14.41$	-1.10	0.551
Metal-rich <sup>b</sup>	$-38.61 \pm 19.16$	-2.02	$15.39 \pm 20.67$	0.745	$-5.92 \pm 19.43$	-0.31	0.123

NOTE—Median age–metallicity–specific orbital energy model coefficients, coefficient uncertainties,  $t$  values, and  $R^2$  values calculated from 100 Monte Carlo iterations for the complete, metal-poor, and metal-rich subsamples (both including and excluding clusters associated with the Sagittarius dSph) assuming all three potentials.

<sup>a</sup>All metal-rich globular clusters

<sup>b</sup>Metal-rich globular clusters excluding those associated with the Sagittarius dSph

1 and 2. In particular, old, metal-rich globular clusters tend to have more negative specific orbital energies and are therefore more tightly bound to the Milky Way than young, metal-poor globular clusters. The metal-poor subsample prefers the full age–metallicity–specific orbital energy relation over any of its nested submodels. These results are independent of assumed potential, although the relationship is much stronger in the McMillan17 potential from McMillan (2017) than either the default or scaled MWPotential2014 potentials from Bovy (2015). We find no clear age–metallicity–specific orbital energy relation in the metal-rich subsample of 10 globular clusters with  $[M/H] > -0.8$  that are not associated with the Sagittarius dSph galaxy. We also find in this metal-rich subsample that an age–metallicity–specific orbital energy relation is not clearly preferred over lower-dimensional models relating age, metallicity, or specific orbital energy.

As we argued in Section 1, accreted metal-rich globular clusters can only be formed in massive dSph galaxies that experience stronger dynamical friction and form their first stars more quickly than lower-mass dSph galaxies. These two properties imply that in a globular

cluster system with many accreted globular clusters, age and metallicity should be correlated with each other but inversely correlated with specific orbital energy. Our observation that old, metal-rich globular clusters are more tightly bound to the Milky Way than young, metal-poor globular clusters confirms the importance of accretion for the formation of the Milky Way’s globular cluster system. Our inference also supports previous proposals that a large fraction of the Milky Way’s metal-poor globular clusters were accreted (e.g., Forbes & Bridges 2010; Forbes 2020; Kruijssen et al. 2019a,b, 2020; Masari et al. 2019; Trujillo-Gomez et al. 2021).

All but two of the metal rich clusters in our sample have tightly bound orbits and old ages, broadly consistent with an in situ origin for metal-rich globular clusters. These two clusters—Terzan 7 and Pal 12—are both young and on energetic orbits. They have been securely associated with the Sagittarius dSph galaxy though, and therefore have been accreted (e.g., Law & Majewski 2010; Sohn et al. 2018). Because we do not observe a strong age–metallicity–specific orbital energy for metal-rich globular clusters unassociated with the Sagittarius dSph, our inferences do not support an accretion origin

**Table 4.** Median Model Comparison  $F$  Statistics

Sample	$H_0 : \beta_\tau = 0$		$H_0 : \beta_M = 0$		$H_0 : \beta_\tau = \beta_M = 0$	
	$F$	$p$	$F$	$p$	$F$	$p$
<b>Default MWPotential2014</b>						
Complete	2.63	$1.1 \times 10^{-1}$	3.27	$7.2 \times 10^{-2}$	2.38	$1.0 \times 10^{-1}$
Metal-poor	5.71	$2.1 \times 10^{-2}$	4.66	$3.7 \times 10^{-2}$	3.58	$3.7 \times 10^{-2}$
Metal-rich <sup>a</sup>	0.11	$7.5 \times 10^{-1}$	0.85	$3.8 \times 10^{-1}$	0.43	$6.6 \times 10^{-1}$
Metal-rich <sup>b</sup>	3.19	$1.1 \times 10^{-1}$	0.85	$3.9 \times 10^{-1}$	1.62	$2.6 \times 10^{-1}$
<b>Scaled MWPotential2014</b>						
Complete	2.17	$1.5 \times 10^{-1}$	4.40	$4.1 \times 10^{-2}$	2.65	$8.0 \times 10^{-2}$
Metal-poor	6.44	$1.5 \times 10^{-2}$	5.12	$2.9 \times 10^{-2}$	4.00	$2.6 \times 10^{-2}$
Metal-rich <sup>a</sup>	0.00	$9.8 \times 10^{-1}$	1.27	$2.9 \times 10^{-1}$	0.68	$5.3 \times 10^{-1}$
Metal-rich <sup>b</sup>	4.78	$6.5 \times 10^{-1}$	0.93	$3.7 \times 10^{-1}$	2.40	$1.6 \times 10^{-1}$
<b>McMillan17</b>						
Complete	32.05	$5.9 \times 10^{-7}$	20.13	$3.8 \times 10^{-5}$	20.81	$2.0 \times 10^{-7}$
Metal-poor	20.89	$4.2 \times 10^{-5}$	16.38	$2.2 \times 10^{-4}$	12.90	$4.3 \times 10^{-5}$
Metal-rich <sup>a</sup>	11.00	$9.0 \times 10^{-3}$	1.20	$3.0 \times 10^{-1}$	5.52	$3.0 \times 10^{-2}$
Metal-rich <sup>b</sup>	0.55	$4.8 \times 10^{-1}$	0.09	$7.7 \times 10^{-1}$	0.49	$6.3 \times 10^{-1}$

NOTE— $F$  statistics and associated  $p$  values comparing the full three parameter age–metallicity–specific orbital energy relation derived for each potential to all possible lower-dimensional submodels. The large  $F$  statistics and small  $p$  values indicate that the full age–metallicity–specific orbital energy relation is superior to all lower-dimensional nested models for the metal-poor subsample.

<sup>a</sup>All metal-rich globular clusters

<sup>b</sup>Metal-rich globular clusters excluding those associated with the Sagittarius dSph

for most metal-rich globular clusters. As there are only 10 metal-rich clusters unassociated with the Sagittarius dSph in our sample, we are unable to choose between gas-rich mergers or formation in gas-rich disks for the origin of the Milky Way’s metal-rich globular clusters.

In our analysis, we used relative ages from Marín-Franch et al. (2009) calculated assuming the Carretta & Gratton (1997) metallicity scale and the theoretical model grid from Dotter et al. (2007). To ensure that our results are insensitive to the assumed metallicity scale or theoretical model grid underlying the Marín-Franch et al. (2009) age inferences, we performed the same analysis using all of the relative ages from Marín-Franch et al. (2009) calculated assuming both the Zinn & West (1984) and Carretta & Gratton (1997) metallicity scales and all of the Bertelli et al. (1994), Girardi et al. (2000), Pietrinferni et al. (2004), and Dotter et al. (2007) theoretical model grids. In all cases, our analysis produces the same trends with comparable statistical significance. This should not be surprising, as Marín-Franch et al. (2009) found that their relative ages inferences were insensitive to their choice of metallicity scale

or theoretical model grid. This consistency supports the robustness of our findings.

As a consequence of the simple physical explanation we outline to explain the age–metallicity–specific orbital energy relation we observe in the Milky Way’s globular cluster system, we predict that the globular cluster systems of other  $L^*$  galaxies should evince similar relations. That is, we predict that other  $L^*$  galaxies in isolation or in low-density group environments like the Local Group should have globular cluster systems in which old, metal-rich globular clusters have more negative specific orbital energies and are therefore more tightly bound to their host halo than young, metal-poor globular clusters. We argue that this is a natural outcome of galaxy formation in a  $\Lambda$ CDM universe.

While we infer the importance of accretion for the origin of the Milky Way’s globular cluster system from an analysis of its ensemble properties, our approach cannot associate individual globular clusters with individual accretion events. Detailed simulations of Milky Way analogs have shown how a globular cluster systems properties can be used to reveal that halo’s accretion history

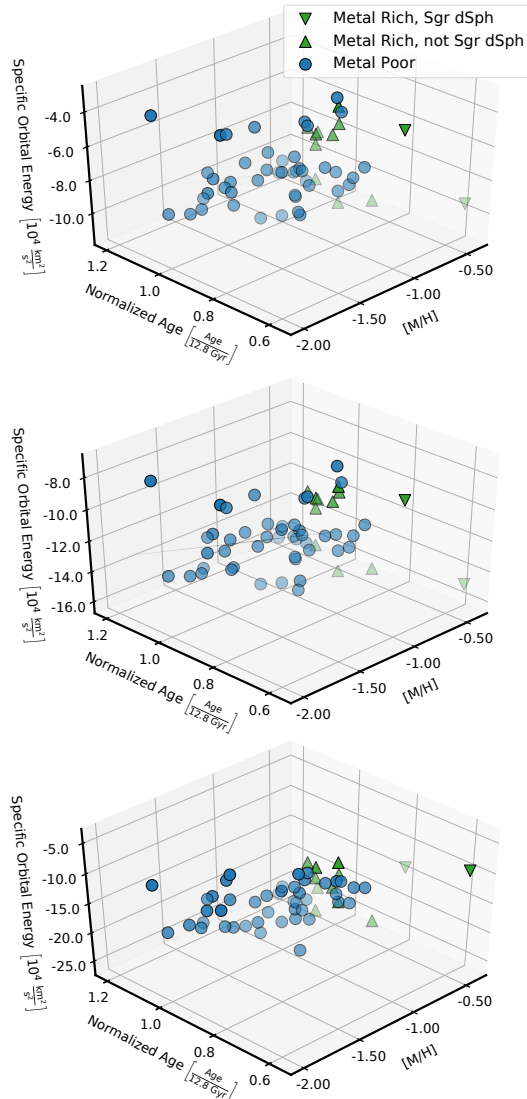


**Figure 1.** Age–metallicity–specific orbital energy distribution of the Milky Way globular clusters listed in Tables 1 and 2. We plot metal-poor clusters with  $[M/H] \leq -0.8$  as blue circles and metal-rich clusters with  $[M/H] > -0.8$  as green triangles. Downward-pointing triangles are metal-rich clusters associated with the Sagittarius dSph galaxy, while upward-pointing triangles are metal-rich clusters unassociated with the Sagittarius dSph galaxy. Each plot is looking down the plane defined by the median best-fit age–metallicity–specific orbital energy relation for the metal-poor subsample as reported in Table 3. Top: specific orbital energies calculated assuming the default `MWPotential2014` potential from Bovy (2015). Middle: specific orbital energies calculated assuming the scaled `MWPotential2014` potential. Bottom: specific orbital energies calculated assuming the `McMillan17` potential from McMillan (2017). It is visually clear in the `McMillan17` potential that the metal-poor subsample lies in a plane in age–metallicity–specific orbital energy space as indicated by the highly significant coefficients  $\beta_\tau$  and  $\beta_M$  listed in Table 3 and the small  $F$  test  $p$  values listed in Table 4.

(e.g., Kruijssen et al. 2019a,b, 2020; Pfeffer et al. 2020; Trujillo-Gomez et al. 2021). When applied to the Milky Way, that formalism can quantify the properties of massive satellite galaxies that have since merged with the Milky Way (e.g., Myeong et al. 2018; Hughes et al. 2019; Kruijssen et al. 2019b, 2020; Pfeffer et al. 2020; Trujillo-Gomez et al. 2021). Moreover, efforts have been made to match the kinematics of clusters to stellar streams

associated with known accretion events. For example, Massari et al. (2019) employed this technique in combination with in-group age–metallicity relations to assign candidate accreted globular clusters to specific progenitors. However, our analysis shows that it is beneficial to use similar techniques on the entire cluster population, thereby capturing the general imprint that accretion has



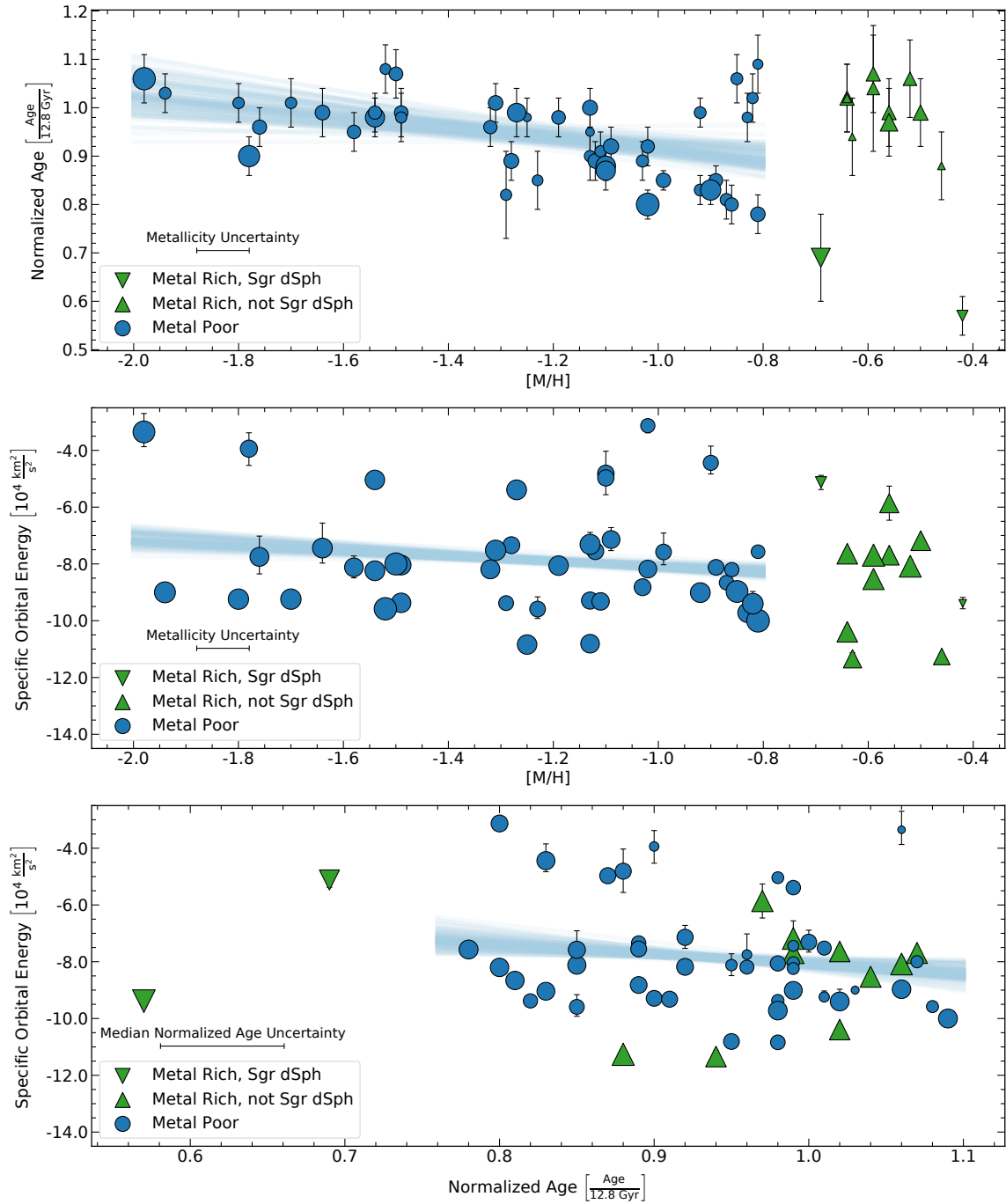


**Figure 2.** Two-dimensional projections of the age–metallicity–specific orbital energy distribution of the 57 Milky Way globular clusters listed in Tables 1 and 2 assuming the default `MWPotential2014` potential (Bovy 2015). We plot metal-poor clusters as blue circles and metal-rich clusters as green triangles. Downward-pointing triangles are metal-rich clusters associated with the Sagittarius dSph galaxy, while upward-pointing triangles are metal-rich clusters unassociated with the Sagittarius dSph galaxy. The sizes of the points corresponds to the relative values of the suppressed axis. In blue we indicate the two-dimensional projections of the best-fit age–metallicity–specific orbital energy relation in the metal-poor subsample for each of the 100 Monte Carlo trials. Top: metallicity–age relation. Middle: metallicity–specific orbital energy relation. Bottom: age–specific orbital energy relation.

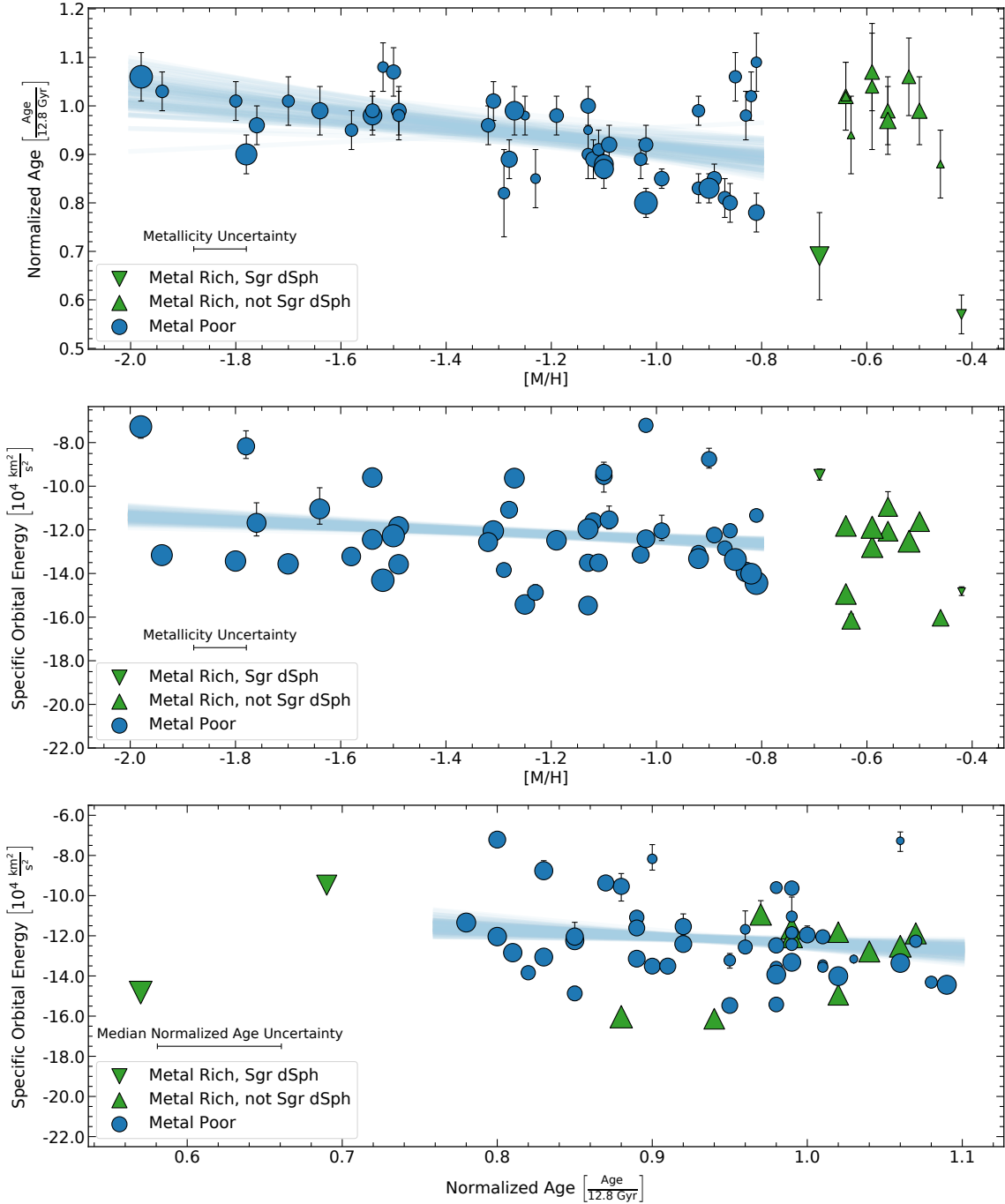


**Figure 3.** Two-dimensional projections of the age–metallicity–specific orbital energy distribution of the 57 Milky Way globular clusters listed in Tables 1 and 2 assuming the scaled `MWPotential2014` potential. We plot metal-poor clusters as blue circles and metal-rich clusters as green triangles. Downward-pointing triangles are metal-rich clusters associated with the Sagittarius dSph galaxy, while upward-pointing triangles are metal-rich clusters unassociated with the Sagittarius dSph galaxy. The sizes of the points corresponds to the relative values of the suppressed axis. In blue we indicate the two-dimensional projections of the best-fit age–metallicity–specific orbital energy relation in the metal-poor subsample for each of the 100 Monte Carlo trials. Top: metallicity–age relation. Middle: metallicity–specific orbital energy relation. Bottom: age–specific orbital energy relation.

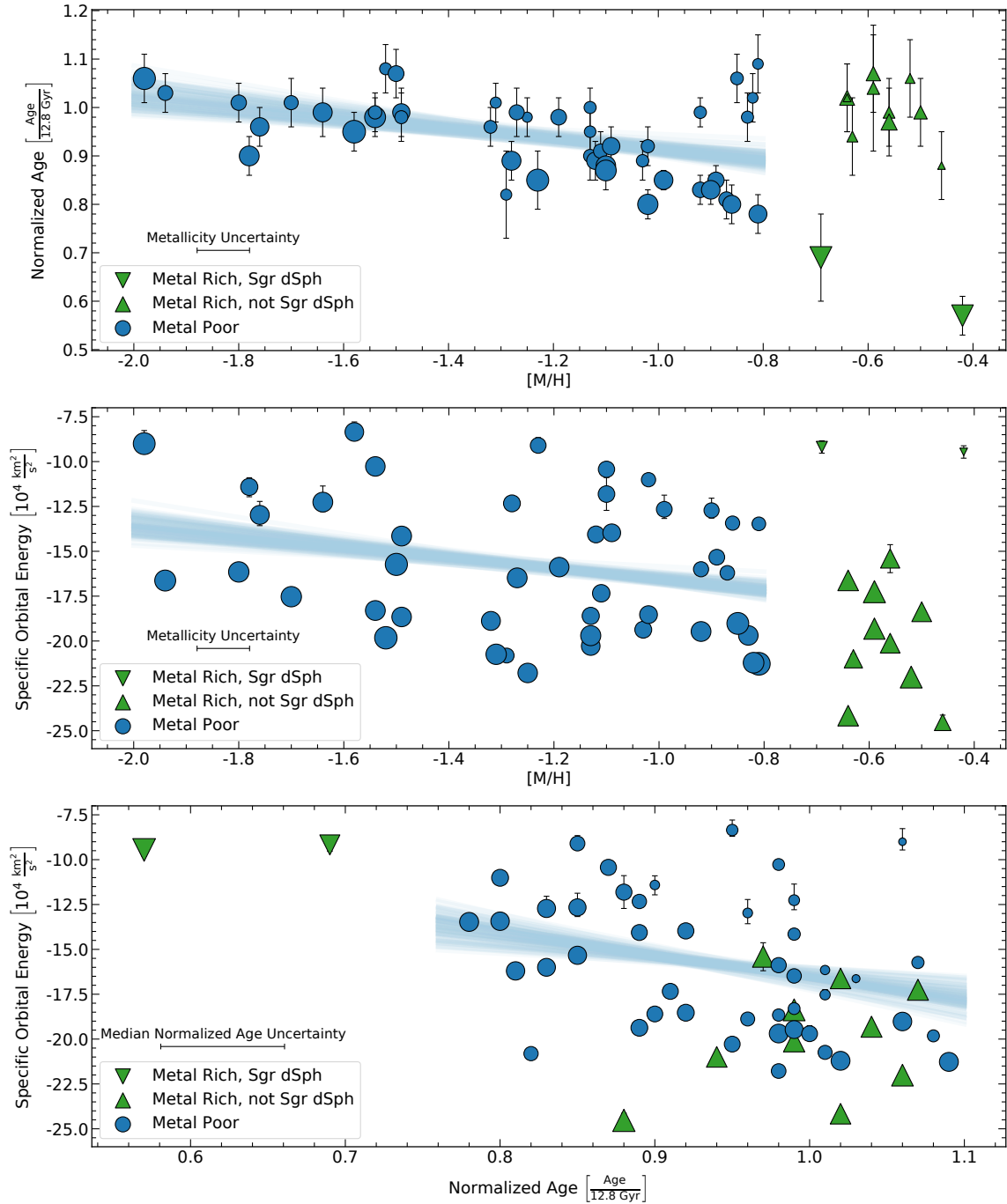


**Figure 4.** Two-dimensional projections of the age–metallicity–specific orbital energy distribution of the 57 Milky Way globular clusters listed in Tables 1 and 2 assuming McMillan17 potential (McMillan 2017). We plot metal-poor clusters as blue circles and metal-rich clusters as green triangles. Downward-pointing triangles are metal-rich clusters associated with the Sagittarius dSph galaxy, while upward-pointing triangles are metal-rich clusters unassociated with the Sagittarius dSph galaxy. The sizes of the points corresponds to the relative values of the suppressed axis. In blue we indicate the two-dimensional projections of the best-fit age–metallicity–specific orbital energy relation in the metal-poor subsample for each of the 100 Monte Carlo trials. Top: metallicity–age relation. Middle: metallicity–specific orbital energy relation. Bottom: age–specific orbital energy relation.

**Table 5.** Median Model Comparison BIC Statistics

Sample	Full Model	$\beta_\tau = 0$	$\beta_M = 0$	$\beta_\tau = \beta_M = 0$
<b>Default MWPotential2014</b>				
Complete	241	240	240	238
Metal-poor	188	190	189	188
Metal-rich <sup>a</sup>	55	53	54	52
Metal-rich <sup>b</sup>	43	44	41	42
<b>Scaled MWPotential2014</b>				
Complete	247	245	248	244
Metal-poor	192	194	193	192
Metal-rich <sup>a</sup>	57	54	56	53
Metal-rich <sup>b</sup>	42	45	41	43
<b>McMillan17</b>				
Complete	302	324	316	326
Metal-poor	236	251	247	250
Metal-rich <sup>a</sup>	69	76	68	74
Metal-rich <sup>b</sup>	55	54	53	52

NOTE—BIC values comparing the full three parameter age–metallicity–specific orbital energy relation derived for each potential to all possible lower-dimensional submodels. The small BIC values indicate that the full age–metallicity–specific orbital energy relation is superior to all lower-dimensional nested models for both the complete sample and its metal-poor subsample in the McMillan17 potential.

<sup>a</sup> All metal-rich globular clusters

<sup>b</sup> Metal-rich globular clusters excluding those associated with the Sagittarius dSph

had on the Milky Way’s globular cluster system’s age–metallicity–specific orbital energy relation.

Because proper motions are more difficult to infer for distant clusters, our input sample lacks outer halo clusters. This bias is unlikely to affect our conclusion, as the only plausible explanation for weakly bound outer halo clusters is accretion from dwarf galaxies. Our input sample also lacks highly extincted disk and bulge clusters. This bias is unlikely to affect our conclusion either, as disk/bulge clusters are metal-rich and would not appear in our metal-poor subsample even if they were present in our input sample.

The age–metallicity–specific orbital energy relation we observe in our metal-poor subsample of globular clusters is much stronger in the McMillan17 potential than in the MWPotential2014 potential. As discussed in Section 3, the default MWPotential2014 potential represents a comparatively smaller, lower-mass Milky Way than the McMillan17 potential. In addition, the more massive McMillan17 potential appears to be a better match to Gaia DR2-informed Milky Way virial mass inferences. Under the default MWPotential2014 potential, most of the weakly bound clusters are relatively less bound than

they are in the McMillan17 potential, though this difference is diminished in the scaled MWPotential2014. This results in a relatively larger spread in orbital energy, which might explain the weaker age–metallicity–specific orbital energy relation. Nevertheless, the age–metallicity–specific orbital energy relation has the same form in all three potentials and we are confident its existence is robust to the choice of potential.

## 5. CONCLUSION

We find that in the metal-poor subsample of 45 Milky Way globular clusters with  $[M/H] \leq -0.8$  in Tables 1 and 2, relatively young or metal-poor globular clusters are weakly bound to the Milky Way, while relatively old or metal-rich globular clusters are tightly bound to the Galaxy. We argue that this relationship is naturally explained by the accretion of globular clusters from now-disrupted dwarf galaxies. We propose that this observation is a consequence of the combined effects of the stellar mass–metallicity relationship for dwarf galaxies, the dependence of dynamical friction on mass, and the relationship between a galaxy’s dynamical time and its central density. Accreted metal-rich globular clusters can only form in massive dSph galaxies that can attain high metallicities and will be strongly affected by dynamical friction. These more massive dSph galaxies capable of forming metal-rich clusters will also produce their oldest stellar populations before lower-mass dSph galaxies that form in lower  $\sigma$  peaks in the universe’s primordial matter density distribution. These lower-mass dSph galaxies will be much less affected by dynamical friction and can only produce low-metallicity globular clusters. Because these properties are independent of the specific accretion history of the Milky Way, we assert that they are a natural outcome of galaxy formation in a  $\Lambda$ CDM universe. We predict that the globular cluster systems of other  $L^*$  galaxies in isolation or in low-density groups like the Local Group will lie in a plane in age–metallicity–specific orbital energy space.

## ACKNOWLEDGMENTS

We thank Brendan Griffen and David Nataf for insightful suggestions that improved our analyses. This work has made use of data from the European Space Agency (ESA) mission Gaia (<https://www.cosmos.esa.int/gaia>), processed by the Gaia Data Processing and Analysis Consortium (DPAC, <https://www.cosmos.esa.int/web/gaia/dpac/consortium>). Funding for the DPAC has been provided by national institutions, in particular the institutions participating in the Gaia Multilateral Agreement. This research has made use of NASA’s Astrophysics Data System Bibliographic Services. This research has made use of the SIMBAD database, operated at CDS, Strasbourg, France (Wenger et al. 2000). This research has made use of the VizieR catalogue access tool, CDS, Strasbourg, France. The original description of the VizieR service was published in A&AS 143, 23 (Ochsenbein et al. 2000).

*Software:* `galpy` (Bovy 2015), `numpy` (van der Walt et al. 2011), `pandas` (McKinney 2010), `statsmodels` (Seabold & Perktold 2010)



## REFERENCES

- Arenou, F., Luri, X., Babusiaux, C., et al. 2018, *A&A*, 616, A17
- Ashman, K. M., & Zepf, S. E. 1992, *ApJ*, 384, 50
- Baumgardt, H., Hilker, M., Sollima, A., & Bellini, A. 2019, *MNRAS*, 482, 5138
- Bertelli, G., Bressan, A., Chiosi, C., Fagotto, F., & Nasi, E. 1994, *A&AS*, 106, 275
- Binney, J., & Tremaine, S. 2008, *Galactic Dynamics: Second Edition*
- Bjork, S. R., & Chaboyer, B. 2006, *ApJ*, 641, 1102
- Bland-Hawthorn, J., & Gerhard, O. 2016, *ARA&A*, 54, 529
- Bovy, J. 2015, *ApJS*, 216, 29
- Buonanno, R., Corsi, C. E., Castellani, M., et al. 1999, *AJ*, 118, 1671
- Buonanno, R., Corsi, C. E., Zinn, R., et al. 1998, *ApJL*, 501, L33
- Carretta, E., Bragaglia, A., Gratton, R. G., et al. 2014, *A&A*, 561, A87
- Carretta, E., & Gratton, R. G. 1997, *A&AS*, 121, 95
- Carretta, E., Bragaglia, A., Gratton, R. G., et al. 2010, *A&A*, 520, A95
- Chaboyer, B., Fenton, W. H., Nelan, J. E., Patnaude, D. J., & Simon, F. E. 2001, *ApJ*, 562, 521
- Choksi, N., Gnedin, O. Y., & Li, H. 2018, *MNRAS*, 480, 2343
- Chou, M.-Y., Majewski, S. R., Cunha, K., et al. 2007, *ApJ*, 670, 346
- Cohen, J. G. 2004, *AJ*, 127, 1545
- Crowley, C., Kohley, R., Hambly, N. C., et al. 2016, *A&A*, 595, A6
- Dotter, A., Chaboyer, B., Jevremović, D., et al. 2007, *AJ*, 134, 376
- Eadie, G., & Jurić, M. 2019, *The Astrophysical Journal*, 875, 159
- Erkal, D., Belokurov, V., Laporte, C. F. P., et al. 2019, *MNRAS*, 487, 2685
- Fabricius, C., Bastian, U., Portell, J., et al. 2016, *A&A*, 595, A3
- Forbes, D. A. 2020, *MNRAS*, 493, 847
- Forbes, D. A., & Bridges, T. 2010, *MNRAS*, 404, 1203
- Forbes, D. A., Bastian, N., Gieles, M., et al. 2018, *Proceedings of the Royal Society of London Series A*, 474, 20170616
- Gaia Collaboration, Prusti, T., de Bruijne, J. H. J., et al. 2016, *A&A*, 595, A1
- Gaia Collaboration, Helmi, A., van Leeuwen, F., et al. 2018a, *A&A*, 616, A12
- Gaia Collaboration, Brown, A. G. A., Vallenari, A., et al. 2018b, *A&A*, 616, A1
- Girardi, L., Bressan, A., Bertelli, G., & Chiosi, C. 2000, *A&AS*, 141, 371
- Gravity Collaboration, Abuter, R., Amorim, A., et al. 2018, *A&A*, 615, L15
- Griffen, B. F., Drinkwater, M. J., Thomas, P. A., Helly, J. C., & Pimblet, K. A. 2010, *MNRAS*, 405, 375
- Hambly, N. C., Cropper, M., Boudreault, S., et al. 2018, *A&A*, 616, A15
- Harris, W. E. 1996, *AJ*, 112, 1487
- Hasselquist, S., Shetrone, M., Smith, V., et al. 2017, *ApJ*, 845, 162
- Hughes, M. E., Pfeffer, J., Martig, M., et al. 2019, *MNRAS*, 482, 2795
- Jurić, M., Ivezić, Ž., Brooks, A., et al. 2008, *ApJ*, 673, 864
- Keller, B. W., Kruijssen, J. M. D., Pfeffer, J., et al. 2020, *MNRAS*, 495, 4248
- Kim, J.-h., Ma, X., Grudić, M. Y., et al. 2018, *MNRAS*, 474, 4232
- Kirby, E. N., Cohen, J. G., Guhathakurta, P., et al. 2013, *ApJ*, 779, 102
- Kravtsov, A. V., & Gnedin, O. Y. 2005, *ApJ*, 623, 650
- Kruijssen, J. M. D. 2015, *MNRAS*, 454, 1658
- . 2019, *MNRAS*, 486, L20
- Kruijssen, J. M. D., Pfeffer, J. L., Crain, R. A., & Bastian, N. 2019a, *MNRAS*, 486, 3134
- Kruijssen, J. M. D., Pfeffer, J. L., Reina-Campos, M., Crain, R. A., & Bastian, N. 2019b, *MNRAS*, 486, 3180
- Kruijssen, J. M. D., Pfeffer, J. L., Chevance, M., et al. 2020, *MNRAS*, 498, 2472
- Larsen, S. S., Brodie, J. P., & Strader, J. 2012, *A&A*, 546, A53
- Law, D. R., & Majewski, S. R. 2010, *ApJ*, 714, 229
- Leaman, R., VandenBerg, D. A., & Mendel, J. T. 2013, *MNRAS*, 436, 122
- Letarte, B., Hill, V., Jablonka, P., et al. 2006, *A&A*, 453, 547
- Li, H., & Gnedin, O. Y. 2014, *ApJ*, 796, 10
- . 2019, *MNRAS*, 486, 4030
- Lindgren, L., Hernández, J., Bombrun, A., et al. 2018, *A&A*, 616, A2
- Luri, X., Brown, A. G. A., Sarro, L. M., et al. 2018, *A&A*, 616, A9
- Mackey, A. D., & Gilmore, G. F. 2004, *MNRAS*, 355, 504
- Marín-Franch, A., Aparicio, A., Piotto, G., et al. 2009, *ApJ*, 694, 1498
- Massari, D., Koppelman, H. H., & Helmi, A. 2019, *A&A*, 630, L4
- McKinney, W. 2010, in *Proceedings of the 9th Python in Science Conference (SciPy)*

- McMillan, P. J. 2017, *MNRAS*, 465, 76
- Miyamoto, M., & Nagai, R. 1975, *PASJ*, 27, 533
- Mo, H., van den Bosch, F. C., & White, S. 2010, *Galaxy Formation and Evolution*
- Mottini, M., Wallerstein, G., & McWilliam, A. 2008, *AJ*, 136, 614
- Muratov, A. L., & Gnedin, O. Y. 2010, *ApJ*, 718, 1266
- Myeong, G. C., Evans, N. W., Belokurov, V., Sanders, J. L., & Koposov, S. E. 2018, *ApJL*, 863, L28
- Navarro, J. F., Frenk, C. S., & White, S. D. M. 1996, *ApJ*, 462, 563
- Ochsenbein, F., Bauer, P., & Marcout, J. 2000, *A&AS*, 143, 23
- Pascale, R., Posti, L., Nipoti, C., & Binney, J. 2018, *MNRAS*, 480, 927
- Patel, S. G., van Dokkum, P. G., Franx, M., et al. 2013a, *ApJ*, 766, 15
- Patel, S. G., Fumagalli, M., Franx, M., et al. 2013b, *ApJ*, 778, 115
- Pfeffer, J., Kruijssen, J. M. D., Crain, R. A., & Bastian, N. 2018, *MNRAS*, 475, 4309
- Pfeffer, J. L., Trujillo-Gomez, S., Kruijssen, J. M. D., et al. 2020, *MNRAS*, 499, 4863
- Pietrinferni, A., Cassisi, S., Salaris, M., & Castelli, F. 2004, *ApJ*, 612, 168
- Renaud, F., Agertz, O., & Gieles, M. 2017, *MNRAS*, 465, 3622
- Rutledge, G. A., Hesser, J. E., & Stetson, P. B. 1997a, *PASP*, 109, 907
- Rutledge, G. A., Hesser, J. E., Stetson, P. B., et al. 1997b, *PASP*, 109, 883
- Sbordone, L., Bonifacio, P., Buonanno, R., et al. 2007, *A&A*, 465, 815
- Schönrich, R., Binney, J., & Dehnen, W. 2010, *MNRAS*, 403, 1829
- Seabold, S., & Perktold, J. 2010, in *9th Python in Science Conference*
- Searle, L., & Zinn, R. 1978, *ApJ*, 225, 357
- Simon, J. D. 2019, *ARA&A*, 57, 375
- Sohn, S. T., Watkins, L. L., Fardal, M. A., et al. 2018, *ApJ*, 862, 52
- Trujillo-Gomez, S., Kruijssen, J. M. D., Reina-Campos, M., et al. 2021, *MNRAS*, 503, 31
- van der Walt, S., Colbert, S. C., & Varoquaux, G. 2011, *Computing in Science and Engineering*, 13, 22
- VandenBerg, D. A., Brogaard, K., Leaman, R., & Casagrande, L. 2013, *ApJ*, 775, 134
- Vasiliev, E., & Belokurov, V. 2020, *MNRAS*, 497, 4162
- Wagner-Kaiser, R., Mackey, D., Sarajedini, A., et al. 2017, *MNRAS*, 471, 3347
- Wang, W., Han, J., Cautun, M., Li, Z., & Ishigaki, M. N. 2020, *Science China Physics, Mechanics, and Astronomy*, 63, 109801
- Wenger, M., Ochsenbein, F., Egret, D., et al. 2000, *A&AS*, 143, 9
- West, M. J., Côté, P., Marzke, R. O., & Jordán, A. 2004, *Nature*, 427, 31
- Wright, E. L. 2006, *PASP*, 118, 1711
- Zinn, R., & West, M. J. 1984, *ApJS*, 55, 45

Table 1. Input Astrometric, Distance, and Radial Velocity Data

NGC	Alternate	$\alpha$	$\delta$	$\mu_\alpha$	$\mu_\delta$	$\varpi$	$\sigma_{\alpha\delta}$	$\sigma_{\alpha\varpi}$	$\sigma_{\delta\varpi}$	$d$	$v_r$
Name	Name	[deg]	[deg]	[mas yr $^{-1}$ ]	[mas yr $^{-1}$ ]	[mas]				[kpc]	[km s $^{-1}$ ]
NGC 104	47 Tuc	6.0194	-72.0821	5.2477 $^{+0.0016}_{-0.0016}$	-2.5189 $^{+0.0015}_{-0.0015}$	0.1959 $^{+0.0002}_{-0.0002}$	-0.06	-0.01	-0.01	4.3 $^{+0.1}_{-0.1}$	-18.7 $^{+0.2}_{-0.2}$
NGC 288	...	13.1879	-26.5858	4.2385 $^{+0.0035}_{-0.0035}$	-5.6470 $^{+0.0026}_{-0.0026}$	0.1401 $^{+0.0021}_{-0.0021}$	0.25	0.15	-0.13	8.1 $^{+0.2}_{-0.2}$	-46.6 $^{+0.4}_{-0.4}$
NGC 362	...	15.8099	-70.8489	6.6954 $^{+0.0045}_{-0.0045}$	-2.5184 $^{+0.0034}_{-0.0034}$	0.0788 $^{+0.0012}_{-0.0012}$	-0.09	-0.04	-0.12	8.3 $^{+0.2}_{-0.2}$	223.5 $^{+0.5}_{-0.5}$
NGC 1261	...	48.067543	-55.216224	1.6900 $^{+0.0400}_{-0.0400}$	-2.1100 $^{+0.0400}_{-0.0400}$	...	...	...	...	16.0 $^{+0.4}_{-0.4}$	68.2 $^{+4.6}_{-4.6}$
NGC 1851	...	78.528	-40.0456	2.1308 $^{+0.0037}_{-0.0037}$	-0.6220 $^{+0.0040}_{-0.0040}$	0.0298 $^{+0.0011}_{-0.0011}$	-0.09	0.06	-0.07	12.2 $^{+0.3}_{-0.3}$	320.9 $^{+1.0}_{-1.0}$
NGC 2298	...	102.2464	-36.0046	3.2762 $^{+0.0060}_{-0.0060}$	-2.1913 $^{+0.0061}_{-0.0061}$	0.0791 $^{+0.0019}_{-0.0019}$	0.07	0.08	-0.07	10.6 $^{+0.2}_{-0.2}$	148.9 $^{+1.2}_{-1.2}$
NGC 2808	...	138.0071	-64.8645	1.0032 $^{+0.0032}_{-0.0032}$	0.2785 $^{+0.0032}_{-0.0032}$	0.0560 $^{+0.0006}_{-0.0006}$	-0.08	0.05	-0.01	9.3 $^{+0.2}_{-0.2}$	93.6 $^{+2.4}_{-2.4}$
NGC 3201	...	154.3987	-46.4125	8.3344 $^{+0.0021}_{-0.0021}$	-1.9895 $^{+0.0020}_{-0.0020}$	0.1724 $^{+0.0006}_{-0.0006}$	0.12	0.04	-0.02	5.1 $^{+0.1}_{-0.1}$	494.0 $^{+0.2}_{-0.2}$
NGC 4147	...	182.52626	18.542638	-1.7800 $^{+0.0400}_{-0.0400}$	-2.1000 $^{+0.0400}_{-0.0400}$	...	...	...	...	18.8 $^{+0.4}_{-0.4}$	183.2 $^{+0.7}_{-0.7}$
NGC 4590	M 68	189.8651	-26.7454	-2.7640 $^{+0.0050}_{-0.0050}$	1.7916 $^{+0.0039}_{-0.0039}$	0.0664 $^{+0.0025}_{-0.0025}$	-0.29	-0.0	0.13	10.1 $^{+0.2}_{-0.2}$	-95.2 $^{+0.4}_{-0.4}$
NGC 4833	...	194.8978	-70.8718	-8.3147 $^{+0.0036}_{-0.0036}$	-0.9366 $^{+0.0029}_{-0.0029}$	0.1163 $^{+0.0010}_{-0.0010}$	0.06	0.05	0.11	5.9 $^{+0.1}_{-0.1}$	200.2 $^{+1.2}_{-1.2}$
NGC 5024	M 53	198.2262	18.1661	-0.1466 $^{+0.0045}_{-0.0045}$	-1.3514 $^{+0.0032}_{-0.0032}$	0.0143 $^{+0.0018}_{-0.0018}$	-0.28	-0.12	0.08	18.4 $^{+0.4}_{-0.4}$	-79.1 $^{+4.1}_{-4.1}$
NGC 5053	...	199.1124	17.7008	-0.3591 $^{+0.0071}_{-0.0071}$	-1.2586 $^{+0.0048}_{-0.0048}$	0.0064 $^{+0.0040}_{-0.0040}$	-0.32	0.13	-0.17	16.2 $^{+0.4}_{-0.4}$	44.0 $^{+0.4}_{-0.4}$
NGC 5139	$\omega$ Cen	201.7876	-47.4515	-3.1925 $^{+0.0022}_{-0.0022}$	-6.7445 $^{+0.0019}_{-0.0019}$	0.1237 $^{+0.0011}_{-0.0011}$	-0.03	-0.04	0.17	5.1 $^{+0.1}_{-0.1}$	232.3 $^{+0.5}_{-0.5}$
NGC 5272	M 3	205.5486	28.376	-0.1127 $^{+0.0029}_{-0.0029}$	-2.6274 $^{+0.0022}_{-0.0022}$	0.0265 $^{+0.0010}_{-0.0010}$	-0.03	-0.01	-0.05	10.0 $^{+0.2}_{-0.2}$	-148.6 $^{+0.4}_{-0.4}$
NGC 5286	...	206.6136	-51.3723	0.1836 $^{+0.0076}_{-0.0076}$	-0.1477 $^{+0.0068}_{-0.0068}$	0.0168 $^{+0.0025}_{-0.0025}$	-0.01	-0.02	0.08	10.7 $^{+0.2}_{-0.2}$	58.3 $^{+3.2}_{-3.2}$
NGC 5466	...	211.3614	28.5331	-5.4044 $^{+0.0042}_{-0.0042}$	-0.7907 $^{+0.0041}_{-0.0041}$	0.0210 $^{+0.0021}_{-0.0021}$	0.07	0.04	0.15	16.6 $^{+0.4}_{-0.4}$	107.7 $^{+0.3}_{-0.3}$
NGC 5904	M 5	229.6394	2.0766	4.0613 $^{+0.0032}_{-0.0032}$	-9.8610 $^{+0.0029}_{-0.0029}$	0.1135 $^{+0.0010}_{-0.0010}$	0.03	-0.07	0.09	7.3 $^{+0.2}_{-0.2}$	52.1 $^{+0.5}_{-0.5}$
NGC 5927	...	232.0065	-50.6694	-5.0470 $^{+0.0060}_{-0.0060}$	-3.2325 $^{+0.0055}_{-0.0055}$	0.0996 $^{+0.0021}_{-0.0021}$	-0.08	-0.0	-0.01	7.4 $^{+0.2}_{-0.2}$	-115.7 $^{+3.1}_{-3.1}$
NGC 5986	...	236.5211	-37.7826	-4.2217 $^{+0.0084}_{-0.0084}$	-4.5515 $^{+0.0065}_{-0.0065}$	0.0718 $^{+0.0031}_{-0.0031}$	-0.18	-0.1	-0.01	10.3 $^{+0.2}_{-0.2}$	88.9 $^{+3.7}_{-3.7}$
NGC 6093	M 80	244.2564	-22.9723	-2.9469 $^{+0.0090}_{-0.0090}$	-5.5613 $^{+0.0073}_{-0.0073}$	0.0558 $^{+0.0030}_{-0.0030}$	0.01	-0.1	0.06	8.7 $^{+0.2}_{-0.2}$	9.3 $^{+3.1}_{-3.1}$
NGC 6121	M 4	245.8976	-26.5279	-12.4956 $^{+0.0033}_{-0.0033}$	-18.9789 $^{+0.0030}_{-0.0030}$	0.5001 $^{+0.0007}_{-0.0007}$	0.08	-0.08	0.03	2.2 $^{+0.1}_{-0.1}$	70.2 $^{+0.3}_{-0.3}$
NGC 6101	...	246.450485	-72.202194	1.7300 $^{+0.0500}_{-0.0500}$	-0.4700 $^{+0.0500}_{-0.0500}$	...	...	...	...	15.1 $^{+0.3}_{-0.3}$	361.4 $^{+1.7}_{-1.7}$
NGC 6144	...	246.8061	-26.0301	-1.7646 $^{+0.0085}_{-0.0085}$	-2.6371 $^{+0.0063}_{-0.0063}$	0.0668 $^{+0.0040}_{-0.0040}$	0.08	-0.15	0.15	10.1 $^{+0.2}_{-0.2}$	188.9 $^{+1.1}_{-1.1}$
NGC 6171	M 107	248.135	-13.057	-1.9359 $^{+0.0064}_{-0.0064}$	-5.9487 $^{+0.0048}_{-0.0048}$	0.1480 $^{+0.0026}_{-0.0026}$	0.03	-0.13	0.17	6.3 $^{+0.1}_{-0.1}$	-33.8 $^{+0.3}_{-0.3}$
NGC 6205	M 13	250.4217	36.4596	-3.1762 $^{+0.0027}_{-0.0027}$	-2.5876 $^{+0.0030}_{-0.0030}$	0.0801 $^{+0.0007}_{-0.0007}$	0.19	-0.04	0.04	7.0 $^{+0.2}_{-0.2}$	-246.6 $^{+0.9}_{-0.9}$
NGC 6218	M 12	251.8101	-1.951	-0.1577 $^{+0.0040}_{-0.0040}$	-6.7683 $^{+0.0027}_{-0.0027}$	0.1563 $^{+0.0013}_{-0.0013}$	0.29	-0.06	0.11	4.7 $^{+0.1}_{-0.1}$	-42.1 $^{+0.6}_{-0.6}$
NGC 6254	M 10	254.2861	-4.0981	-4.7031 $^{+0.0039}_{-0.0039}$	-6.5285 $^{+0.0027}_{-0.0027}$	0.1511 $^{+0.0014}_{-0.0014}$	0.21	-0.07	0.1	4.3 $^{+0.1}_{-0.1}$	75.8 $^{+1.0}_{-1.0}$
NGC 6304	...	258.637	-29.4816	-3.9478 $^{+0.0095}_{-0.0095}$	-1.1248 $^{+0.0069}_{-0.0069}$	0.1077 $^{+0.0034}_{-0.0034}$	0.16	-0.04	0.13	6.0 $^{+0.1}_{-0.1}$	-107.3 $^{+3.6}_{-3.6}$
NGC 6341	M 92	259.2821	43.1352	-4.9367 $^{+0.0040}_{-0.0040}$	-0.5559 $^{+0.0040}_{-0.0040}$	0.0564 $^{+0.0008}_{-0.0008}$	0.11	-0.04	-0.0	8.1 $^{+0.2}_{-0.2}$	-121.6 $^{+1.5}_{-1.5}$
NGC 6352	...	261.3739	-48.427	-2.1859 $^{+0.0066}_{-0.0066}$	-4.4209 $^{+0.0036}_{-0.0036}$	0.1543 $^{+0.0018}_{-0.0018}$	0.22	-0.12	0.13	5.6 $^{+0.1}_{-0.1}$	-120.9 $^{+3.0}_{-3.0}$
NGC 6366	...	261.9393	-5.0752	-0.3835 $^{+0.0054}_{-0.0054}$	-5.1309 $^{+0.0044}_{-0.0044}$	0.2292 $^{+0.0022}_{-0.0022}$	0.27	-0.08	0.14	3.6 $^{+0.1}_{-0.1}$	-122.3 $^{+0.5}_{-0.5}$
NGC 6362	...	262.9772	-67.0492	-5.5014 $^{+0.0028}_{-0.0028}$	-4.7417 $^{+0.0032}_{-0.0032}$	0.0974 $^{+0.0011}_{-0.0011}$	0.06	-0.06	0.06	7.5 $^{+0.2}_{-0.2}$	-13.1 $^{+0.6}_{-0.6}$
NGC 6388	...	264.0654	-44.7423	-1.3548 $^{+0.0072}_{-0.0072}$	-2.7144 $^{+0.0061}_{-0.0061}$	0.0482 $^{+0.0034}_{-0.0034}$	0.11	-0.12	0.18	11.5 $^{+0.3}_{-0.3}$	81.2 $^{+1.2}_{-1.2}$
NGC 6397	...	265.1697	-53.6773	3.2908 $^{+0.0026}_{-0.0026}$	-17.5908 $^{+0.0025}_{-0.0025}$	0.3781 $^{+0.0007}_{-0.0007}$	0.1	-0.05	0.07	2.2 $^{+0.1}_{-0.1}$	18.9 $^{+0.1}_{-0.1}$

Table 1 continued

Table 1 (continued)

NGC	Alternate	$\alpha$	$\delta$	$\mu_\alpha$	$\mu_\delta$	$\varpi$	$\sigma_{\alpha\delta}$	$\sigma_{\alpha\varpi}$	$\sigma_{\delta\varpi}$	$d$	$v_r$
Name	Name	[deg]	[deg]	[mas yr <sup>-1</sup> ]	[mas yr <sup>-1</sup> ]	[mas]				[kpc]	[km s <sup>-1</sup> ]
NGC 6441	...	267.5540	-37.066	-2.5394 <sup>+0.0070</sup>	-5.3010 <sup>+0.0057</sup>	0.0403 <sup>+0.0037</sup>	0.17	-0.18	0.17	9.7 <sup>+0.2</sup>	18.3 <sup>+1.7</sup>
NGC 6496	...	269.7677	-44.2660	-3.0290 <sup>+0.0057</sup>	-9.1971 <sup>+0.0050</sup>	0.0803 <sup>+0.0031</sup>	0.07	-0.15	0.17	11.6 <sup>+0.3</sup>	-112.7 <sup>+5.7</sup>
NGC 6535	...	270.959	-0.2953	-4.2101 <sup>+0.0115</sup>	-2.9461 <sup>+0.0108</sup>	0.1294 <sup>+0.0047</sup>	0.1	0.1	-0.02	6.8 <sup>+0.2</sup>	-215.1 <sup>+0.5</sup>
NGC 6541	...	271.9827	-43.7144	0.2762 <sup>+0.0054</sup>	-8.7659 <sup>+0.0048</sup>	0.1139 <sup>+0.0025</sup>	-0.03	-0.04	0.08	7.4 <sup>+0.2</sup>	-156.2 <sup>+2.7</sup>
NGC 6584	...	274.656646	-52.215778	-0.0500 <sup>+0.0100</sup>	-7.2200 <sup>+0.0100</sup>	...	-0.15	...	...	13.0 <sup>+0.3</sup>	222.9 <sup>+15.0</sup>
NGC 6637	M 69	277.8342	-32.3565	-5.0669 <sup>+0.0104</sup>	-5.8017 <sup>+0.0094</sup>	0.0746 <sup>+0.0032</sup>	0.23	-0.01	-0.05	8.2 <sup>+0.2</sup>	39.9 <sup>+2.8</sup>
NGC 6656	M 22	279.1048	-23.9102	9.8019 <sup>+0.0036</sup>	-5.5643 <sup>+0.0034</sup>	0.2602 <sup>+0.0009</sup>	0.15	-0.05	0.02	3.2 <sup>+0.1</sup>	-148.9 <sup>+0.4</sup>
NGC 6681	M 70	280.802	-32.2892	1.3853 <sup>+0.0076</sup>	-4.7174 <sup>+0.0065</sup>	0.1096 <sup>+0.0038</sup>	0.26	-0.24	0.1	8.7 <sup>+0.2</sup>	218.6 <sup>+1.2</sup>
NGC 6723	...	284.888123	-36.632248	1.0000 <sup>+0.0100</sup>	-2.4200 <sup>+0.0100</sup>	...	0.11	...	...	8.6 <sup>+0.2</sup>	-94.5 <sup>+3.6</sup>
NGC 6752	...	287.7175	-59.9833	-3.1908 <sup>+0.0018</sup>	-4.0347 <sup>+0.0020</sup>	0.2310 <sup>+0.0011</sup>	0.19	-0.29	0.03	3.9 <sup>+0.1</sup>	-24.5 <sup>+1.9</sup>
NGC 6779	M 56	289.148	30.184	-2.0092 <sup>+0.0051</sup>	1.6553 <sup>+0.0056</sup>	0.0702 <sup>+0.0015</sup>	0.03	-0.05	-0.03	9.9 <sup>+0.2</sup>	-135.7 <sup>+0.8</sup>
Terzan 7	...	289.432983	-34.657722	-3.0400 <sup>+0.0600</sup>	-1.7100 <sup>+0.0500</sup>	...	...	...	...	23.0 <sup>+0.5</sup>	166.0 <sup>+4.0</sup>
Arp 2	...	292.183807	-30.355638	-2.4000 <sup>+0.0400</sup>	-1.5400 <sup>+0.0300</sup>	...	...	...	...	27.6 <sup>+0.6</sup>	115.0 <sup>+10.0</sup>
NGC 6809	M 55	295.0046	-30.9621	-3.4017 <sup>+0.0031</sup>	-9.2642 <sup>+0.0028</sup>	0.1707 <sup>+0.0011</sup>	0.18	-0.03	0.0	5.3 <sup>+0.1</sup>	174.8 <sup>+0.4</sup>
Terzan 8	...	295.435028	-33.999474	-2.9100 <sup>+0.0800</sup>	-1.6300 <sup>+0.0600</sup>	...	...	...	...	25.4 <sup>+0.6</sup>	130.0 <sup>+8.0</sup>
NGC 6838	M 71	298.4427	18.779	-3.3842 <sup>+0.0027</sup>	-2.6528 <sup>+0.0028</sup>	0.2252 <sup>+0.0010</sup>	0.11	-0.11	-0.01	3.8 <sup>+0.1</sup>	-22.9 <sup>+0.2</sup>
NGC 6934	...	308.547393	7.404472	-2.6700 <sup>+0.0400</sup>	-4.5200 <sup>+0.0500</sup>	...	...	...	...	15.2 <sup>+0.3</sup>	-411.4 <sup>+1.6</sup>
NGC 6981	M 72	313.3662	-12.5386	-1.2488 <sup>+0.0089</sup>	-3.3117 <sup>+0.0068</sup>	0.0225 <sup>+0.0063</sup>	0.26	-0.38	-0.13	16.8 <sup>+0.4</sup>	-345.1 <sup>+3.7</sup>
NGC 7078	M 15	322.4949	12.1661	-0.6238 <sup>+0.0041</sup>	-3.7960 <sup>+0.0039</sup>	0.0568 <sup>+0.0014</sup>	-0.04	-0.02	-0.15	10.2 <sup>+0.2</sup>	-107.5 <sup>+0.3</sup>
NGC 7089	M 2	323.3497	-0.8177	3.4911 <sup>+0.0077</sup>	-2.1501 <sup>+0.0071</sup>	0.0591 <sup>+0.0035</sup>	-0.04	-0.14	-0.14	11.4 <sup>+0.3</sup>	-5.3 <sup>+2.0</sup>
NGC 7099	M 30	325.0888	-23.1792	-0.7017 <sup>+0.0063</sup>	-7.2218 <sup>+0.0055</sup>	0.0746 <sup>+0.0040</sup>	0.3	-0.29	-0.27	7.9 <sup>+0.2</sup>	-184.2 <sup>+1.0</sup>
Pal 12	...	326.661804	-21.252611	-3.0600 <sup>+0.0500</sup>	-3.3200 <sup>+0.0500</sup>	...	...	...	...	18.7 <sup>+0.4</sup>	27.8 <sup>+1.5</sup>

NOTE—Input globular cluster astrometry, distance, and radial velocity data. While most cluster astrometric data come from *Gaia* Collaboration et al. (2018a), the data for NGC 6584 and NGC 6723 come from Baumgardt et al. (2019) while the data for NGC 1261, NGC 4147, NGC 6101, Terzan 7, Arp 2, Terzan 8, NGC 6934, and Pal 12 come from Sohn et al. (2018). Distance and radial velocity data come from the December 2010 revision of the Harris (1996) compilation.

Table 2. Age, Metallicity, and Specific Orbital Energy Inferences

NGC Name	Alternate Name	$\tau$	[M/H]	SOE <sub>MW14</sub> [ $10^4 \text{ km}^2 \text{ s}^{-2}$ ]	SOE <sub>Sca1edMW14</sub> [ $10^4 \text{ km}^2 \text{ s}^{-2}$ ]	SOE <sub>Mc17</sub> [ $10^4 \text{ km}^2 \text{ s}^{-2}$ ]
NGC 104	47 Tuc	1.02 <sup>+0.07</sup> <sub>-0.07</sub>	-0.64 <sup>+0.05</sup> <sub>-0.05</sub>	-7.64 <sup>+0.06</sup> <sub>-0.05</sub>	-11.82 <sup>+0.05</sup> <sub>-0.05</sub>	-16.62 <sup>+0.05</sup> <sub>-0.05</sub>
NGC 288	...	0.83 <sup>+0.03</sup> <sub>-0.03</sub>	-0.92 <sup>+0.05</sup> <sub>-0.05</sub>	-9.04 <sup>+0.08</sup> <sub>-0.04</sub>	-13.06 <sup>+0.07</sup> <sub>-0.05</sub>	-16.00 <sup>+0.11</sup> <sub>-0.07</sub>
NGC 362	...	0.81 <sup>+0.04</sup> <sub>-0.04</sub>	-0.87 <sup>+0.05</sup> <sub>-0.05</sub>	-8.66 <sup>+0.16</sup> <sub>-0.18</sub>	-12.84 <sup>+0.17</sup> <sub>-0.17</sub>	-16.20 <sup>+0.17</sup> <sub>-0.20</sub>
NGC 1261	...	0.80 <sup>+0.04</sup> <sub>-0.04</sub>	-0.86 <sup>+0.05</sup> <sub>-0.05</sub>	-8.20 <sup>+0.07</sup> <sub>-0.06</sub>	-12.04 <sup>+0.06</sup> <sub>-0.08</sub>	-13.43 <sup>+0.13</sup> <sub>-0.09</sub>
NGC 1851	...	0.78 <sup>+0.04</sup> <sub>-0.04</sub>	-0.81 <sup>+0.05</sup> <sub>-0.05</sub>	-7.57 <sup>+0.15</sup> <sub>-0.10</sub>	-11.34 <sup>+0.14</sup> <sub>-0.09</sub>	-13.47 <sup>+0.14</sup> <sub>-0.09</sub>
NGC 2298	...	0.99 <sup>+0.05</sup> <sub>-0.05</sub>	-1.49 <sup>+0.05</sup> <sub>-0.05</sub>	-8.04 <sup>+0.19</sup> <sub>-0.10</sub>	-11.85 <sup>+0.17</sup> <sub>-0.13</sub>	-14.15 <sup>+0.22</sup> <sub>-0.15</sub>
NGC 2808	...	0.85 <sup>+0.03</sup> <sub>-0.03</sub>	-0.89 <sup>+0.05</sup> <sub>-0.05</sub>	-8.12 <sup>+0.08</sup> <sub>-0.07</sub>	-12.24 <sup>+0.13</sup> <sub>-0.08</sub>	-15.33 <sup>+0.11</sup> <sub>-0.10</sub>
NGC 3201	...	0.80 <sup>+0.03</sup> <sub>-0.03</sub>	-1.02 <sup>+0.05</sup> <sub>-0.05</sub>	-3.13 <sup>+0.19</sup> <sub>-0.25</sub>	-7.21 <sup>+0.19</sup> <sub>-0.25</sub>	-11.01 <sup>+0.23</sup> <sub>-0.26</sub>
NGC 4147	...	0.89 <sup>+0.04</sup> <sub>-0.04</sub>	-1.28 <sup>+0.05</sup> <sub>-0.05</sub>	-7.34 <sup>+0.04</sup> <sub>-0.04</sub>	-11.08 <sup>+0.06</sup> <sub>-0.04</sub>	-12.33 <sup>+0.11</sup> <sub>-0.09</sub>
NGC 4590	M 68	0.90 <sup>+0.04</sup> <sub>-0.04</sub>	-1.78 <sup>+0.05</sup> <sub>-0.05</sub>	-3.94 <sup>+0.56</sup> <sub>-0.59</sub>	-8.17 <sup>+0.71</sup> <sub>-0.56</sub>	-11.41 <sup>+0.51</sup> <sub>-0.55</sub>
NGC 4833	...	0.98 <sup>+0.05</sup> <sub>-0.05</sub>	-1.49 <sup>+0.05</sup> <sub>-0.05</sub>	-9.37 <sup>+0.10</sup> <sub>-0.09</sub>	-13.58 <sup>+0.08</sup> <sub>-0.08</sub>	-18.66 <sup>+0.12</sup> <sub>-0.11</sub>
NGC 5024	M 53	0.99 <sup>+0.05</sup> <sub>-0.05</sub>	-1.64 <sup>+0.05</sup> <sub>-0.05</sub>	-7.44 <sup>+0.88</sup> <sub>-0.53</sub>	-11.04 <sup>+0.97</sup> <sub>-0.70</sub>	-12.26 <sup>+0.90</sup> <sub>-0.53</sub>
NGC 5053	...	0.96 <sup>+0.04</sup> <sub>-0.04</sub>	-1.76 <sup>+0.05</sup> <sub>-0.05</sub>	-7.75 <sup>+0.73</sup> <sub>-0.60</sub>	-11.68 <sup>+0.92</sup> <sub>-0.60</sub>	-12.97 <sup>+0.75</sup> <sub>-0.60</sub>
NGC 5139	$\omega$ Cen	0.90 <sup>+0.05</sup> <sub>-0.05</sub>	-1.13 <sup>+0.05</sup> <sub>-0.05</sub>	-9.29 <sup>+0.11</sup> <sub>-0.06</sub>	-13.51 <sup>+0.07</sup> <sub>-0.08</sub>	-18.60 <sup>+0.12</sup> <sub>-0.07</sub>
NGC 5272	M 3	0.89 <sup>+0.04</sup> <sub>-0.04</sub>	-1.12 <sup>+0.05</sup> <sub>-0.05</sub>	-7.55 <sup>+0.13</sup> <sub>-0.12</sub>	-11.61 <sup>+0.13</sup> <sub>-0.12</sub>	-14.06 <sup>+0.13</sup> <sub>-0.12</sub>
NGC 5286	...	0.98 <sup>+0.04</sup> <sub>-0.04</sub>	-1.19 <sup>+0.05</sup> <sub>-0.05</sub>	-8.06 <sup>+0.07</sup> <sub>-0.08</sub>	-12.48 <sup>+0.11</sup> <sub>-0.07</sub>	-15.88 <sup>+0.16</sup> <sub>-0.13</sub>
NGC 5466	...	1.06 <sup>+0.05</sup> <sub>-0.05</sub>	-1.98 <sup>+0.05</sup> <sub>-0.05</sub>	-3.35 <sup>+0.65</sup> <sub>-0.52</sub>	-7.27 <sup>+0.44</sup> <sub>-0.53</sub>	-9.00 <sup>+0.73</sup> <sub>-0.46</sub>
NGC 5904	M 5	0.83 <sup>+0.03</sup> <sub>-0.03</sub>	-0.90 <sup>+0.05</sup> <sub>-0.05</sub>	-4.44 <sup>+0.59</sup> <sub>-0.39</sub>	-8.76 <sup>+0.50</sup> <sub>-0.41</sub>	-12.72 <sup>+0.68</sup> <sub>-0.43</sub>
NGC 5927	...	0.99 <sup>+0.07</sup> <sub>-0.07</sub>	-0.50 <sup>+0.05</sup> <sub>-0.05</sub>	-7.18 <sup>+0.09</sup> <sub>-0.10</sub>	-11.62 <sup>+0.10</sup> <sub>-0.09</sub>	-18.37 <sup>+0.10</sup> <sub>-0.07</sub>
NGC 5986	...	0.95 <sup>+0.04</sup> <sub>-0.04</sub>	-1.13 <sup>+0.05</sup> <sub>-0.05</sub>	-10.81 <sup>+0.19</sup> <sub>-0.16</sub>	-15.47 <sup>+0.21</sup> <sub>-0.12</sub>	-20.28 <sup>+0.29</sup> <sub>-0.22</sub>
NGC 6093	M 80	0.98 <sup>+0.04</sup> <sub>-0.04</sub>	-1.25 <sup>+0.05</sup> <sub>-0.05</sub>	-10.84 <sup>+0.07</sup> <sub>-0.05</sub>	-15.42 <sup>+0.08</sup> <sub>-0.07</sub>	-21.78 <sup>+0.17</sup> <sub>-0.12</sub>
NGC 6121	M 4	0.98 <sup>+0.05</sup> <sub>-0.05</sub>	-0.83 <sup>+0.05</sup> <sub>-0.05</sub>	-9.72 <sup>+0.02</sup> <sub>-0.01</sub>	-13.93 <sup>+0.02</sup> <sub>-0.01</sub>	-19.69 <sup>+0.05</sup> <sub>-0.04</sub>
NGC 6101	...	0.98 <sup>+0.04</sup> <sub>-0.04</sub>	-1.54 <sup>+0.05</sup> <sub>-0.05</sub>	-5.04 <sup>+0.13</sup> <sub>-0.11</sub>	-9.60 <sup>+0.13</sup> <sub>-0.11</sub>	-10.27 <sup>+0.22</sup> <sub>-0.26</sub>
NGC 6144	...	1.08 <sup>+0.05</sup> <sub>-0.05</sub>	-1.52 <sup>+0.05</sup> <sub>-0.05</sub>	-9.58 <sup>+0.18</sup> <sub>-0.18</sub>	-14.31 <sup>+0.15</sup> <sub>-0.13</sub>	-19.82 <sup>+0.18</sup> <sub>-0.20</sub>

Table 2 continued



Table 2 (continued)

NGC	Alternate	$\tau$	[M/H]	SOE <sub>MW14</sub>	SOE <sub>ScaledMW14</sub>	SOE <sub>Mct17</sub>
Name	Name			[ $10^4 \text{ km}^2 \text{ s}^{-2}$ ]	[ $10^4 \text{ km}^2 \text{ s}^{-2}$ ]	[ $10^4 \text{ km}^2 \text{ s}^{-2}$ ]
NGC 6171	M 107	1.09 <sup>+0.06</sup> <sub>-0.06</sub>	-0.81 <sup>+0.05</sup> <sub>-0.05</sub>	-10.00 <sup>+0.09</sup> <sub>-0.09</sub>	-14.44 <sup>+0.08</sup> <sub>-0.07</sub>	-21.27 <sup>+0.11</sup> <sub>-0.08</sub>
NGC 6205	M 13	0.91 <sup>+0.04</sup> <sub>-0.04</sub>	-1.11 <sup>+0.05</sup> <sub>-0.05</sub>	-9.32 <sup>+0.10</sup> <sub>-0.07</sub>	-13.51 <sup>+0.11</sup> <sub>-0.05</sub>	-17.34 <sup>+0.11</sup> <sub>-0.08</sub>
NGC 6218	M 12	0.99 <sup>+0.03</sup> <sub>-0.03</sub>	-0.92 <sup>+0.05</sup> <sub>-0.05</sub>	-9.01 <sup>+0.15</sup> <sub>-0.18</sub>	-13.32 <sup>+0.18</sup> <sub>-0.19</sub>	-19.47 <sup>+0.17</sup> <sub>-0.20</sub>
NGC 6254	M 10	0.89 <sup>+0.04</sup> <sub>-0.04</sub>	-1.03 <sup>+0.05</sup> <sub>-0.05</sub>	-8.82 <sup>+0.10</sup> <sub>-0.08</sub>	-13.14 <sup>+0.11</sup> <sub>-0.07</sub>	-19.37 <sup>+0.12</sup> <sub>-0.08</sub>
NGC 6304	...	1.06 <sup>+0.08</sup> <sub>-0.08</sub>	-0.52 <sup>+0.05</sup> <sub>-0.05</sub>	-8.08 <sup>+0.23</sup> <sub>-0.21</sub>	-12.52 <sup>+0.22</sup> <sub>-0.22</sub>	-22.01 <sup>+0.27</sup> <sub>-0.34</sub>
NGC 6341	M 92	1.03 <sup>+0.04</sup> <sub>-0.04</sub>	-1.94 <sup>+0.05</sup> <sub>-0.05</sub>	-9.00 <sup>+0.10</sup> <sub>-0.11</sub>	-13.16 <sup>+0.13</sup> <sub>-0.10</sub>	-16.63 <sup>+0.09</sup> <sub>-0.11</sub>
NGC 6352	...	0.99 <sup>+0.07</sup> <sub>-0.07</sub>	-0.56 <sup>+0.05</sup> <sub>-0.05</sub>	-7.69 <sup>+0.17</sup> <sub>-0.15</sub>	-12.06 <sup>+0.13</sup> <sub>-0.19</sub>	-20.12 <sup>+0.18</sup> <sub>-0.16</sub>
NGC 6366	...	1.04 <sup>+0.13</sup> <sub>-0.13</sub>	-0.59 <sup>+0.05</sup> <sub>-0.05</sub>	-8.53 <sup>+0.19</sup> <sub>-0.10</sub>	-12.78 <sup>+0.15</sup> <sub>-0.11</sub>	-19.31 <sup>+0.20</sup> <sub>-0.10</sub>
NGC 6362	...	1.06 <sup>+0.05</sup> <sub>-0.05</sub>	-0.85 <sup>+0.05</sup> <sub>-0.05</sub>	-8.97 <sup>+0.08</sup> <sub>-0.07</sub>	-13.36 <sup>+0.07</sup> <sub>-0.09</sub>	-19.02 <sup>+0.09</sup> <sub>-0.11</sub>
NGC 6388	...	0.94 <sup>+0.08</sup> <sub>-0.08</sub>	-0.63 <sup>+0.05</sup> <sub>-0.05</sub>	-11.34 <sup>+0.21</sup> <sub>-0.16</sub>	-16.13 <sup>+0.27</sup> <sub>-0.18</sub>	-20.99 <sup>+0.26</sup> <sub>-0.29</sub>
NGC 6397	...	0.99 <sup>+0.04</sup> <sub>-0.04</sub>	-1.54 <sup>+0.05</sup> <sub>-0.05</sub>	-8.24 <sup>+0.04</sup> <sub>-0.06</sub>	-12.44 <sup>+0.05</sup> <sub>-0.06</sub>	-18.30 <sup>+0.04</sup> <sub>-0.06</sub>
NGC 6441	...	0.88 <sup>+0.07</sup> <sub>-0.07</sub>	-0.46 <sup>+0.05</sup> <sub>-0.05</sub>	-11.26 <sup>+0.09</sup> <sub>-0.08</sub>	-16.03 <sup>+0.11</sup> <sub>-0.08</sub>	-24.53 <sup>+0.40</sup> <sub>-0.33</sub>
NGC 6496	...	0.97 <sup>+0.07</sup> <sub>-0.07</sub>	-0.56 <sup>+0.05</sup> <sub>-0.05</sub>	-5.86 <sup>+0.60</sup> <sub>-0.60</sub>	-10.94 <sup>+0.69</sup> <sub>-0.43</sub>	-15.40 <sup>+0.77</sup> <sub>-0.79</sub>
NGC 6535	...	0.82 <sup>+0.09</sup> <sub>-0.09</sub>	-1.29 <sup>+0.05</sup> <sub>-0.05</sub>	-9.38 <sup>+0.09</sup> <sub>-0.09</sub>	-13.84 <sup>+0.12</sup> <sub>-0.11</sub>	-20.81 <sup>+0.08</sup> <sub>-0.08</sub>
NGC 6541	...	1.01 <sup>+0.04</sup> <sub>-0.04</sub>	-1.31 <sup>+0.05</sup> <sub>-0.05</sub>	-7.52 <sup>+0.11</sup> <sub>-0.13</sub>	-12.05 <sup>+0.15</sup> <sub>-0.14</sub>	-20.74 <sup>+0.12</sup> <sub>-0.13</sub>
NGC 6584	...	0.88 <sup>+0.03</sup> <sub>-0.03</sub>	-1.10 <sup>+0.05</sup> <sub>-0.05</sub>	-4.81 <sup>+0.78</sup> <sub>-0.75</sub>	-9.54 <sup>+0.64</sup> <sub>-0.73</sub>	-11.81 <sup>+0.92</sup> <sub>-0.91</sub>
NGC 6637	M 69	1.02 <sup>+0.07</sup> <sub>-0.07</sub>	-0.64 <sup>+0.05</sup> <sub>-0.05</sub>	-10.39 <sup>+0.17</sup> <sub>-0.17</sub>	-14.94 <sup>+0.17</sup> <sub>-0.16</sub>	-24.16 <sup>+0.21</sup> <sub>-0.17</sub>
NGC 6656	M 22	0.99 <sup>+0.05</sup> <sub>-0.05</sub>	-1.27 <sup>+0.05</sup> <sub>-0.05</sub>	-5.39 <sup>+0.15</sup> <sub>-0.16</sub>	-9.63 <sup>+0.19</sup> <sub>-0.19</sub>	-16.48 <sup>+0.15</sup> <sub>-0.17</sub>
NGC 6681	M 70	1.00 <sup>+0.04</sup> <sub>-0.04</sub>	-1.13 <sup>+0.05</sup> <sub>-0.05</sub>	-7.31 <sup>+0.42</sup> <sub>-0.35</sub>	-11.96 <sup>+0.45</sup> <sub>-0.34</sub>	-19.70 <sup>+0.44</sup> <sub>-0.34</sub>
NGC 6723	...	1.02 <sup>+0.05</sup> <sub>-0.05</sub>	-0.82 <sup>+0.05</sup> <sub>-0.05</sub>	-9.40 <sup>+0.43</sup> <sub>-0.27</sub>	-14.01 <sup>+0.42</sup> <sub>-0.29</sub>	-21.21 <sup>+0.49</sup> <sub>-0.35</sub>
NGC 6752	...	0.92 <sup>+0.04</sup> <sub>-0.04</sub>	-1.02 <sup>+0.05</sup> <sub>-0.05</sub>	-8.18 <sup>+0.13</sup> <sub>-0.09</sub>	-12.41 <sup>+0.08</sup> <sub>-0.10</sub>	-18.53 <sup>+0.13</sup> <sub>-0.10</sub>
NGC 6779	M 56	1.07 <sup>+0.05</sup> <sub>-0.05</sub>	-1.50 <sup>+0.05</sup> <sub>-0.05</sub>	-8.00 <sup>+0.17</sup> <sub>-0.14</sub>	-12.27 <sup>+0.16</sup> <sub>-0.16</sub>	-15.73 <sup>+0.17</sup> <sub>-0.17</sub>
Terzan 7	...	0.57 <sup>+0.04</sup> <sub>-0.04</sub>	-0.42 <sup>+0.05</sup> <sub>-0.05</sub>	-9.39 <sup>+0.21</sup> <sub>-0.19</sub>	-14.83 <sup>+0.22</sup> <sub>-0.18</sub>	-9.46 <sup>+0.34</sup> <sub>-0.35</sub>
Arp 2	...	0.85 <sup>+0.06</sup> <sub>-0.06</sub>	-1.23 <sup>+0.05</sup> <sub>-0.05</sub>	-9.59 <sup>+0.43</sup> <sub>-0.33</sub>	-14.87 <sup>+0.35</sup> <sub>-0.33</sub>	-9.10 <sup>+0.44</sup> <sub>-0.36</sub>
NGC 6809	M 55	0.96 <sup>+0.04</sup> <sub>-0.04</sub>	-1.32 <sup>+0.05</sup> <sub>-0.05</sub>	-8.19 <sup>+0.03</sup> <sub>-0.03</sub>	-12.56 <sup>+0.05</sup> <sub>-0.04</sub>	-18.88 <sup>+0.05</sup> <sub>-0.04</sub>
Terzan 8	...	0.95 <sup>+0.04</sup> <sub>-0.04</sub>	-1.58 <sup>+0.05</sup> <sub>-0.05</sub>	-8.12 <sup>+0.40</sup> <sub>-0.37</sub>	-13.22 <sup>+0.34</sup> <sub>-0.39</sub>	-8.35 <sup>+0.56</sup> <sub>-0.35</sub>
NGC 6838	M 71	1.07 <sup>+0.08</sup> <sub>-0.08</sub>	-0.59 <sup>+0.05</sup> <sub>-0.05</sub>	-7.69 <sup>+0.04</sup> <sub>-0.05</sub>	-11.88 <sup>+0.05</sup> <sub>-0.05</sub>	-17.25 <sup>+0.04</sup> <sub>-0.04</sub>

Table 2 continued

Table 2 (continued)

NGC	Alternate	$\tau$	[M/H]	SOE <sub>MW14</sub>	SOE <sub>ScaledMW14</sub>	SOE <sub>Mct17</sub>
Name	Name			[ $10^4 \text{ km}^2 \text{ s}^{-2}$ ]	[ $10^4 \text{ km}^2 \text{ s}^{-2}$ ]	[ $10^4 \text{ km}^2 \text{ s}^{-2}$ ]
NGC 6934	...	$0.87^{+0.04}_{-0.04}$	$-1.10^{+0.05}_{-0.05}$	$-4.97^{+0.20}_{-0.24}$	$-9.37^{+0.22}_{-0.23}$	$-10.43^{+0.33}_{-0.37}$
NGC 6981	M 72	$0.85^{+0.02}_{-0.02}$	$-0.99^{+0.05}_{-0.05}$	$-7.58^{+0.67}_{-0.45}$	$-12.04^{+0.71}_{-0.45}$	$-12.66^{+0.79}_{-0.51}$
NGC 7078	M 15	$1.01^{+0.04}_{-0.04}$	$-1.80^{+0.05}_{-0.05}$	$-9.24^{+0.09}_{-0.06}$	$-13.43^{+0.09}_{-0.06}$	$-16.15^{+0.13}_{-0.13}$
NGC 7089	M 2	$0.92^{+0.04}_{-0.04}$	$-1.09^{+0.05}_{-0.05}$	$-7.14^{+0.42}_{-0.39}$	$-11.54^{+0.63}_{-0.42}$	$-13.97^{+0.38}_{-0.39}$
NGC 7099	M 30	$1.01^{+0.05}_{-0.05}$	$-1.70^{+0.05}_{-0.05}$	$-9.24^{+0.21}_{-0.12}$	$-13.56^{+0.23}_{-0.13}$	$-17.53^{+0.29}_{-0.17}$
Pal 12	...	$0.69^{+0.09}_{-0.09}$	$-0.69^{+0.05}_{-0.05}$	$-5.12^{+0.24}_{-0.26}$	$-9.48^{+0.27}_{-0.24}$	$-9.18^{+0.34}_{-0.35}$

NOTE—Table 2 is ordered by R.A. The first column is normalized age  $\tau = \text{age}/12.8$  Gyr from Marin-Franch et al. (2009) calculated using the Dartmouth Stellar Evolution Program (Chaboyer et al. 2001; Bjork & Chaboyer 2006; Dotter et al. 2007) assuming the metallicities presented in Rutledge et al. (1997a,b) on the Carretta & Gratton (1997) scale. The second column metallicity [M/H] is from Rutledge et al. (1997a,b) on the Carretta & Gratton (1997) scale. The third, fourth, and fifth columns are globular cluster specific orbital energies calculated using the data in Table 1 assuming the default, `MWPotential2014`, the scaled `MWPotential2014` (Bovy 2015), and the `McMillan17` (McMillan 2017) potentials respectively.